BOX 1 | TESTING RESISTANCE OF BACTERIAL CLONES TO MULTIPLE ANTIBIOTICS

● TIMING 1–2 D

1. Draw a grid on the bottom surface of each LB agar plate containing a single or combination of antibiotic(s). Label each square with clone numbers.
2. Pick a single colony from a transformation plate with a single sterile micropipette tip and sequentially streak all the test plates with the tip in the squares assigned to the clone.

▲ CRITICAL STEP The LB plate containing the antibiotic(s) to which the clones are resistant should be streaked last; growth of the bacteria on this last, positive-control plate at Step 4 indicates that the other plates were also inoculated with enough bacteria and incubated for sufficient time.

3. Repeat Step 2 to test the desired number of clones.
4. Incubate all plates at 37 °C for 8–12 h until the bacteria grow on the positive-control plates.
5. Check the growth of each clone on each plate to analyze antibiotic resistance.
6. Store the positive-control plate with the grown bacteria as a master plate at 4 °C for up to 1 month. The master plate is used to set up liquid cultures for plasmid preparation.

▲ CRITICAL STEP *E. coli* strains with an F′ episome must be used for transformation to select destination clones. These strains contain the *ccd*A gene and will survive in the presence of the *ccd*B gene.

▲ CRITICAL STEP Carbenicillin is a more stable analog of ampicillin and can be used interchangeably here and elsewhere in this protocol. As colony formation is slow on LB-carbenicillin+chloramphenicol plates, use LB-carbenicillin plates in this step and test chloramphenicol resistance in Step 18A(xiv).

? TROUBLESHOOTING

(xiv) Test resistance of 8–16 carbenicillin-resistant colonies from Step 18A(xiii) to carbenicillin+chloramphenicol and kanamycin by streaking the bacteria onto LB-kanamycin and LB-carbenicillin+chloramphenicol agar plates (**Box 1**) to select for carbenicillin- and chloramphenicol-resistant and kanamycin-sensitive clones.

▲ CRITICAL STEP Destination vectors should have both ampicillin-resistance and chloramphenicol-resistance genes as schematically shown in **Figures 2c** and **3**. From experience, we have found that some carbenicillin-resistant clones from Step 18A(xiii) are also resistant to kanamycin and contain aberrant plasmids, which can be excluded in this step.

■ PAUSE POINT Store the LB-carbenicillin+chloramphenicol master plates at 4 °C for 1 month until use in the next step.

(xv) Set up separate 2-ml LB-carbenicillin+chloramphenicol liquid cultures for approximately six individual carbenicillin- and chloramphenicol-resistant clones from Step 18A(xiv). Grow at 37 °C in a shaker incubator for 16 h with rocking at maximum speed.

(xvi) Purify the plasmid DNA and check the identity and sequence of the plasmids (see Steps 14–16).

(B) Constructing destination vectors by ligating a promoter fragment to the pDEST-PL vector. ● TIMING **2–3 weeks**

(i) Design and synthesize GSPs for amplifying a promoter fragment (see REAGENT SETUP).

(ii) Prepare the PCR mixture as tabulated below. We usually use PrimeSTAR HS DNA polymerase, but other proofreading polymerases can also be used.

Reagent	Amount per 50 μl reaction	Final concentration/ amount
N2 genomic DNA	200 ng	100–200 ng
Polymerase buffer (5×)	10 μl	1×
dNTP mixture (2.5 mM each)	4 μl	0.2 mM each
Forward GSP (2.5 μM)	5 μl	0.25 μM
Reverse GSP (2.5 μM)	5 μl	0.25 μM
PrimeSTAR HS (2.5 U μl^{-1})	0.5 μl	0.025 U μl^{-1}
ddH_2O	Make up to 50 μl	

(iii) Run the PCR in a thermal cycler using the following parameters:

Cycle	Denature	Anneal	Extend
1	94 °C, 2 min		
2–26 (or up to 31)	98 °C, 10 s	55 °C, 5 s	72 °C, 1 min per kb
Final			72 °C, 5 min

(iv) Verify amplification by running a 5-μl aliquot of the PCR product on a 1% (wt/vol) agarose gel.
(v) Purify the PCR product with PCR-M or by using an equivalent DNA purification column.
(vi) Digest the PCR product and pDEST-PL with appropriate restriction endonucleases.
(vii) Run a 1/20th aliquot of the pDEST-PL digestion mixture on a 1% (wt/vol) agarose gel to confirm the digestion.
(viii) Run the entire digestion mixtures on a 1% (wt/vol) agarose gel and purify the PCR product and digested pDEST-PL with the Wizard SV gel and PCR Clean-Up System or an equivalent gel purification column.
(ix) Run a 1-μl aliquot of the PCR product and digested pDEST-PL together with a DNA ladder on a 1% (wt/vol) agarose gel to estimate the concentration by comparing to the ladder.
■ **PAUSE POINT** Store the purified PCR product and pDEST-PL vector at 4 °C for weeks or at −20 °C for months until use in the next step.
(x) Prepare the ligation mixture as tabulated below in a 1.5-ml microcentrifuge tube and mix well by briefly vortexing or tapping. We usually use the DNA Ligation Kit Ver.2.1, but other ligases can also be used.

Reagent	Amount per 10 μl reaction	Final concentration/ amount
Digested pDEST-PL	50 ng	50 ng
Digested PCR product	50–150 ng	50–150 ng
ddH_2O	Make up to 5 μl	
Solution I (DNA ligation kit)	5 μl	1×

(xi) Incubate the ligation mixture at 16 °C for 1 h or more.
(xii) Transform *E. coli* strain DB3.1 or *ccd*B Survival with 1–3 μl of the ligation mixture by a standard method according to the manufacturer's instructions. Plate-transform the cells on LB-carbenicillin plates and grow at 37 °C overnight to select for carbenicillin-resistant clones.
▲ **CRITICAL STEP** *E. coli* strains with an F′ episome must be used for transformation to select destination clones. These strains contain the *ccd*A gene and will survive in the presence of the *ccd*B gene.
(xiii) Test resistance of the carbenicillin-resistant colonies to chloramphenicol by streaking the bacteria onto LB-carbenicillin+chloramphenicol plates. Optionally, check the insertion of the promoter fragment by performing colony PCR with GoTaq Green Master Mix (or EmeraldAmp PCR Master Mix) following manufacturers' instructions when the insert is >3 kb and the probability of carrying the insert is low.
■ **PAUSE POINT** Master plates can be stored at 4 °C for up to 1 month until use in the next step.
(xiv) Set up separate 2-ml LB-carbenicillin+chloramphenicol liquid cultures for approximately six individual clones resistant to both carbenicillin and chloramphenicol (from Step 18B(xiii)). Grow by rocking vigorously at 37 °C for 16 h.
(xv) Purify the plasmid DNAs and check the identity of the plasmids (see Steps 14–16).

Constructing expression clones ● TIMING **1–2 weeks**

19| Prepare the LR reaction mixture as tabulated below in a 1.5-ml microcentrifuge tube and mix well by briefly vortexing or tapping.

Reagent	Amount per 5 μl reaction
Destination vector (see **Table 2**)	75 ng
Genomic fragment cassette in pENTR-L1-R5	15–100 ng
Fluorescent protein cassette in pENTR-L5-L2	15–100 ng
ddH_2O	Make up to 4 μl
LR Clonase II Plus enzyme mix	1 μl

20| Incubate the LR reaction mixture at 25 °C or at room temperature overnight. Although it is included in the manufacturer's manual for LR Clonase II Plus, we usually omit the proteinase K digestion because we find that its inclusion does not make any difference in the number of colonies obtained in Step 21.

21| Transform *E. coli* strain DH5α (or others) with 1–3 μl of the reaction mixture by a standard method[48]. Plate-transform the cells on LB-carbenicillin plates and grow at 37 °C overnight to select for carbenicillin-resistant clones.
▲ CRITICAL STEP *E. coli* strains with an F′ episome cannot be used to select expression clones. These strains contain the *ccd*A gene and will prevent negative selection with the *ccd*B gene in the destination vectors.
? TROUBLESHOOTING

22| Test the resistance of six to eight carbenicillin-resistant colonies (from Step 21) to chloramphenicol, kanamycin and carbenicillin (**Box 1**) by re-streaking the bacteria on three different LB agar plates, each containing one of the antibiotics, to select for carbenicillin-resistant and chloramphenicol- and kanamycin-sensitive clones.
▲ CRITICAL STEP Expression clones should have the ampicillin-resistance gene and should have neither chloramphenicol- nor kanamycin-resistance genes, as schematically shown in **Figure 2a**. From experience, we have found that some carbenicillin-resistant clones from Step 21 are also resistant to chloramphenicol and/or kanamycin and contain aberrant plasmids, which can be excluded in this step.
■ PAUSE POINT Store the LB-carbenicillin master plates at 4 °C for up to 1 month until use in the next step.

23| Set up separate 2-ml LB-carbenicillin liquid cultures for 2–3 individual carbenicillin-resistant clones from Step 22. Grow by rocking vigorously at 37 °C for 16 h.

24| Purify the plasmid DNAs and check the identity and *att*B1, *att*B2 and *att*B5 sequences of the plasmids (see Steps 14–16).

Generation of transgenic reporter worms by a standard microinjection method ● TIMING **3–4 weeks**
25| Mix a transformation marker DNA, *lin-15*(+), and equal amounts of a pair or a set of reporter minigenes at a total DNA concentration of 100 ng μl^{-1} in 1× injection buffer. We prepare 100 ng μl^{-1} solution for each plasmid DNA, mixing the components in the given ratio.

26| Filter the injection mixture with a centrifugal filter device. We use the Ultrafree-MC Durapore PVDF with a 0.22-μm pore diameter.
■ PAUSE POINT The injection mixture can be stored at 4 °C or at −20 °C for weeks until use in the next step.

27| Inject 20–30 *lin-15*(*n765ts*) adult hermaphrodites grown at 15 °C with the injection mixture.

28| Recover the injected (P_0) worms on an NGM plate at 15 °C overnight.

29| Transfer the P_0 worms to a fresh NGM plate and leave them to lay eggs at 20 °C. Repeat this step twice a day. Culture F_1 worms at 20 °C.

30| Isolate fluorescent or non-Muv F_1 worms and culture them further at 20 °C. As the temperature-sensitive Muv phenotype of the *lin-15*(*n765ts*) mutant is fully penetrant, rescue of the Muv phenotype or expression of the fluorescent proteins in the F_1 generation indicates that the worms carry the injected constructs.

31| Establish transgenic lines that express fluorescent proteins or remain non-Muv at 20 °C for at least 3–5 generations.
■ PAUSE POINT Collect freshly starved worms with M9 buffer in a 2-ml cryotube and leave them in 1× worm freezing solution at room temperature for 30–60 min, and then freeze worms at −80 °C. Worms can be stored for years at −80 °C.
? TROUBLESHOOTING

Checking splicing patterns of minigene-derived mRNAs ● TIMING **2–3 weeks**
32| Harvest well-fed worms of mixed stages from a 90-mm NGM plate with M9 buffer and transfer to a 1.5-ml tube. Wash two to three times with M9 buffer to remove bacteria.

33| Freeze 30–100 μl of the packed worms from Step 32 in liquid nitrogen in a mortar and grind them to powder with a pestle and the mortar. If necessary, occasionally add liquid nitrogen to the mortar to keep the worms frozen.

34| Immediately add 600 µl of RLT buffer (from RNeasy Mini kit) supplemented with 1% (vol/vol) 2-mercaptoethanol to the frozen powder of worms, grind the frozen reagent to powder and continuously mix until thawed.

35| Optionally, shear the suspension with QIAshredder Spin Columns. This step reduces the viscosity of the lysate.

TABLE 6 | Minigene-specific forward and reverse primers.

Primer	Sequence	Use
*att*B1adapterF	See **Table 4**	Minigene-specific forward
GSP-*att*B1F	See **Table 4**	Minigene-specific forward
EGFP#2	5′-TGTGGCCGTTTACGTCG-3′	ECFP/EGFP/venus-specific reverse
EGFP#60-*att*B2R	5′-AGAAAGCTGGGTTTTACTTGTACAGCTCGT-3′	ECFP/EGFP/venus-specific reverse
mRFPseqR	5′-GGAGCCGTACTGGAACTGAG-3′	mRFP1-specific reverse
mRFP#2-*att*B2R	5′-AGAAAGCTGGGTCTTAGGCGCCGGTGGAGT-3′	mRFP1-specific reverse

36| Transfer the homogenate to a 1.5-ml microtube and rock vigorously on a mixer for 5 min at room temperature.
■ **PAUSE POINT** The worm homogenate can be stored at −80 °C for months until use in the next step.

37| Extract total RNA from the worms by using RNeasy Mini and DNase according to the manufacturer's instructions.

38| Check the concentration of extracted total RNA with a NanoVue or an equivalent spectrophotometer.
■ **PAUSE POINT** Total RNA can be stored at −80 °C for months until use in the next step.

39| Verify the quality and quantity of total RNA by running 1–2 µg of total RNA on a 1% (wt/vol) agarose gel after heat denaturation at 70 °C for 5 min. Check integrity of the 28S and 18S ribosomal RNAs by ethidium bromide staining and UV illumination. Run a DNA ladder in the same gel as a marker of size and amount.
▲ **CRITICAL STEP** Ensure that 28S and 18S ribosomal RNAs are extracted without degradation.

40| Perform reverse transcription (RT). We usually use 1–2 µg of total RNA for reverse transcription with the PrimeScript II or Superscript II kits and oligo(dT) primers according to manufacturers' instructions.
■ **PAUSE POINT** The RT product can be stored at −20 °C until use in the next step.

41| Perform PCR using the reaction mixture and reaction conditions tabulated below. We usually use nonproofreading polymerases such as Ex Taq and BIOTAQ. Standard conditions are described below. As transgenic worms carry hundreds of copies of reporter minigenes and are expected to express a high level of minigene-derived mRNAs, 18–22 PCR cycles are sufficient in most cases. We use minigene-specific forward and reverse primers (see **Table 6**) to specifically amplify minigene-derived mRNAs.

Reagent	Amount per 20 µl reaction	Final concentration/ amount
RT reaction mixture	1 µl	
Ex Taq buffer (Mg plus, 10×)	2 µl	1×
dNTP mixture (2.5 mM each)	1.6 µl	0.2 mM each
Forward primer (2.5 µM)	2 µl	0.25 µM
Reverse primer (2.5 µM)	2 µl	0.25 µM
Ex Taq (5 U μl^{-1})	0.2 µl	0.05 U μl^{-1}
ddH_2O	11.2 µl	

Cycle	Denature	Anneal	Extend
1	94 °C, 3 min		
2–19 (or up to 23)	94 °C, 30 s	55 °C, 45 s	72 °C, 1 min per kb
Final			72 °C, 5 min

42| Verify amplification and patterns by running a one-fifth to one-half aliquot of the RT-PCR product on a 1% (wt/vol) agarose gel.

43| To analyze RT-PCR products, directly sequence the purified products, or clone the products in TA-vectors such as pGEM-T Easy, and sequence several clones.

Observation and imaging of cell type–specific alternative splicing patterns ● TIMING **2 d**

44| Paralyze worms on an NGM plate with a drop of 10 mM sodium azide. Observe expression patterns and acquire images of fluorescent proteins in the living transgenic worms with a high-magnification dissection microscope equipped with an epifluorescence system (see EQUIPMENT SETUP).

45| Optionally, observe expression patterns of the fluorescent proteins in single cells with a laser-scanning confocal microscope equipped with DIC optics. A high-magnification view with laser-scanning microscopy will be necessary to look into small tissues or identify cells when analyzing the reporter expression profiles in detail or when fluorescent reporter proteins are unexpectedly localized to subcellular domains.

Integration of extrachromosomal arrays by UV irradiation ● TIMING **3–4 weeks**

46| Culture an extrachromosomal line on a sufficient number of 90-mm NGM plates for >500 well-fed fluorescent young adult worms. Synchronization is not necessary but may be convenient to prepare such a large number of well-fed fluorescent young adult worms.

47| Directly irradiate all the worms on culture plates with 300 J m^{-2} (= 300 × 100 μJ cm^{-2}) UV light (254 nm) with the plate lids open. We use a UV crosslinker that can be preset to monitor the energy of UV to be irradiated.

48| Recover worms at 15 °C with enough food for 3–6 h.

49| Pool P_0 adult hermaphrodites on fresh 90-mm NGM plates using a fluorescence stereoscope. We typically place ten fluorescent and active young-adult hermaphrodites per plate and prepare 10–20 plates. Culture the P_0 worms at 20 °C for 2–3 d.

50| Select 100–200 fluorescent late-larval-stage F_1 worms from the plates in Step 49 and place them individually on separate 35-mm NGM plates. Culture the F_1 worms at 20 °C for 2–3 d.
▲ CRITICAL STEP F_1 worms are heterozygote candidates and should express the fluorescent reporter throughout the body in a promoter-dependent pattern.

51| Screen and select F_1 plates with >75% fully fluorescent F_2 worms by using a fluorescence stereoscope.

52| Isolate 3–5 fully fluorescent F_2 worms individually on separate 35-mm NGM plates, each with a single worm, from each of the F_1 plates selected in Step 51. Culture the F_2 worms at 20 °C for 3–4 d.

53| Screen and select F_2 plates with 100% fully fluorescent progeny using a fluorescence stereoscope. Lines derived from the same F_1 plates should be considered to contain the same integrant alleles.
? TROUBLESHOOTING

EMS mutagenesis and screening ● TIMING **3–4 weeks**

54| Culture a parental strain on a sufficient number (usually 3–5) of 90-mm NGM plates to support the growth of thousands of well-fed adult worms. Synchronization is useful for preparing a large number of worms at one time.

55| Harvest the well-fed worms from NGM plates with M9 buffer and transfer to a 1.5-ml or 15-ml tube. Wash the worms two to three times with M9 buffer to remove bacteria and young larvae. Resuspend the worms in 1 ml of M9 buffer.

56| Add 3 ml of M9 buffer to a 15- to 20-ml glass tube. Add 20 μl of EMS (final concentration 47 mM) and mix completely by swirling.
! CAUTION EMS is carcinogenic. Wear protective clothing and gloves. Avoid breathing vapors, mist or gas. Prepare and use EMS solutions in a fume hood. All EMS-treated labware should be discarded after inactivation with >2 N of NaOH for >24 h in the fume hood.
▲ CRITICAL STEP EMS treatment should be carried out in a glass tube. EMS-treated worms stick to plastic tubes and pipettes, and can be seriously damaged or lost.

57| Add 1 ml of the worm suspension prepared in Step 55 to the glass tube containing M9 buffer and EMS from Step 56. Mix by swirling.

58| Incubate the tube from Step 57 at room temperature for 4 h with occasional swirling.

59| Wash the worms three times with M9 buffer in the glass tube.
! CAUTION All EMS-containing reagents should be discarded after inactivation with >2 N of NaOH for >24 h in a fume hood.

60| Transfer worms to fresh 90-mm NGM plates using a glass pipette.
▲ CRITICAL STEP Use a glass pipette. EMS-treated worms stick to plastic pipettes, and can be seriously damaged or lost.

61| Recover worms at 15 °C for 6–12 h.

62| Pool either P_0 adult hermaphrodites (option A) or F_1 embryos (option B) in fresh 90-mm NGM plates and culture at 15 or 20 °C for 4–8 d until a large number of F_2 worms grow. The more worms are pooled per plate, the earlier the worms on the plate will starve, thus preventing the growth of F_2 worms into adults. Therefore, the number of worms or embryos per plate and the number of plates to be prepared should be optimized and determined for each parent strain according to the expected phenotype of the mutant worms.

(A) Pooling P_0 adult worms

(i) Pick up and transfer about ten gravid P_0 adult hermaphrodites per 90-mm NGM plate from the recovery plates in Step 61. Prepare 50–100 plates and incubate them at 15 or 20 °C until the plates are filled with tens of thousands of F_2 worms. Note that F_1 or F_2 worms are not synchronized with this method and that the worms will be starved when most of the F_2 worms are at larval stages. This option, Step 62A(i), is recommended if the parent worms were not synchronized in Step 54.

(B) Collecting F_1 embryos

(i) Collect P_0 gravid adult hermaphrodites from the recovery plates in Step 61 with M9 buffer and transfer to fresh 90-mm NGM plates.

(ii) Leave the worms at 20 °C to lay eggs for 3–6 h, then remove the P_0 adult worms with M9 buffer and move them to fresh plates. Repeat this step to prepare the required number of plates and incubate them at 15 °C or 20 °C until F_2 worms grow.

(iii) Optionally, if F_2 worms are to be synchronized or grown to adulthood for screening, remove F_1 adult worms after each of them lay tens of eggs by washing out plates with M9 buffer.

63| Screen the F_2 progeny for worms with altered expression profiles of fluorescent proteins under a fluorescence stereoscope equipped with an appropriate dual band-pass filter set (see EQUIPMENT SETUP). Isolate all candidate mutant worms, one worm per NGM plate, and culture for 3–4 d to confirm that the color phenotype is inheritable.
? TROUBLESHOOTING

SNP mapping ● TIMING 2–4 months

64| Cross mutant hermaphrodites with males of the Hawaiian wild-type strain CB4856. We usually cross five L4 mutant hermaphrodites with 10–15 CB4856 males on a spot of 10-μl OP50 liquid culture on a 60-mm NGM plate at 20 °C overnight.

65| Isolate the parental mutant hermaphrodites on individual fresh 60-mm NGM plates. Culture plates at 20 °C for 2–3 d.

66| Pool F_1 L4 hermaphrodites from the plates in Step 65 on fresh 90-mm NGM plates using a fluorescence stereoscope. We place ten F_1 worms per plate and prepare 10–20 plates. Culture plates at 15 or 20 °C for 2 d. Remove F_1 hermaphrodites for use in Step 67 and culture the plates for another 2–4 d.
▲ CRITICAL STEP Pool only crossed F_1 hermaphrodites at L4 stage. Adult F_1 hermaphrodites may be crossed with F_1 males; this will result in contamination of the F_2 generation with males, leading to contamination of F_2 hermaphrodites in Step 68 with sperm from F_2 males. The color phenotype should be suppressed in the crossed F_1 progeny if the mutation is recessive. If all F_1 males, but not hermaphrodites, show the mutant phenotype, the gene is linked to the X chromosome.

67| Transfer F_1 hermaphrodites from Step 66 to fresh 90-mm NGM plates. Culture plates at 20 °C for 4–5 d. This step will roughly synchronize the F_2 generation in Steps 66 and 67 so that F_2 worms can be easily discriminated from the F_3 generation of worms by body size in Step 68.

68| Pick individual F_2 gravid adult worms showing the mutant phenotype from the F_1 pool plates (from Steps 66 and 67) and transfer them into 10 μl of worm lysis solution. We usually use 0.2-ml PCR strip tubes, adding one worm per tube.
▲ CRITICAL STEP Select gravid worms showing an unambiguous mutant phenotype. Contamination with a heterozygous worm will significantly affect the reliability of mapping. Theoretically, 3/16 of F_2 worms will show a recessive color phenotype. Younger worms have fewer germline cells than gravid adults and they contain insufficient genomic DNA for SNP-typing of single worms. Note that mutant worms often grow significantly more slowly than their siblings with heterozygous or wild-type background and may need more time to grow into gravid adults.

69| Lyse the worms at 50 °C for 60 min. Inactivate the lysis buffer at 83 °C for 5 min. We program a thermal cycler to carry out these incubations.

70| Add 30 µl of Tris-EDTA (TE) buffer to the lysate from Step 69 and mix well by pipetting (this yields 40 µl of worm lysate in TE buffer per tube).

71| Repeat Steps 64–70 to obtain enough single-worm lysates from F_2 worms showing a mutant phenotype. With >400 F_2 lysates, the candidate region for mutant phenotypes will be narrowed down to 1–2 Mb.
■ **PAUSE POINT** Single-worm lysates can be stored at 4 °C for weeks until use in subsequent steps.

72| Prepare a pool of the F_2 lysates collected in Steps 70 and 71. We collect 2 µl each from at least 48 single-worm lysates. Note that Steps 72 and 73 are not necessary if the gene of interest is found to be linked to the X chromosome in Steps 64–66.

73| Analyze one or two SNP(s) per chromosome of the pooled lysate from Step 72 to map the chromosome, as described in **Box 2.** Allele names, primers and restriction enzymes for typing SNPs are listed in **Table 7.** Use N2 and CB4856 lysates as controls.

BOX 2 | SINGLE-NUCLEOTIDE POLYMORPHISM (SNP) TYPING ● TIMING 1–2 D

1. Synthesize SNP-typing primers for amplifying a genomic fragment.
2. Prepare the PCR mixture as tabulated below. We use BIOTAQ DNA polymerase, but other proofreading polymerases may also be used.

Reagent	Amount per 10 µl reaction	Final concentration/amount
Single-worm lysate (pool)	3 µl	3/40 ul of 1 worm
NH4 buffer (Mg-free; 10×)	1 µl	1×
$MgCl_2$ (50 mM)	0.5 µl	2.5 mM
dNTP mixture (2.5 mM each)	0.8 µl	0.2 mM each
Primer mixture (1 µM each)	2 µl	0.2 µM each
BIOTAQ DNA Polymerase (5 U $µl^{-1}$)	0.1 µl	0.05 U $µl^{-1}$
ddH_2O	2.6 µl	

▲ **CRITICAL STEP** We recommend testing several available DNA polymerases by typing SNPs of single N2 and CB4856 adult worms according to the method described here before choosing a DNA polymerase for SNP typing.

3. Run the PCR in a thermal cycler using the following parameters:

Cycle	Denature	Anneal	Extend
1	95 °C, 3 min		
2–36	95 °C, 40 s	58 °C, 40 s	72 °C, 40 s
37			72 °C, 7 min

4. Type the SNPs by either restriction fragment length polymorphism (RFLP) analysis (A) or by direct sequencing (B).

(A) SNP typing by RFLP analysis

(i) Premix the digestion mixture as tabulated below.

Reagent	Amount per reaction	Final concentration/amount
Restriction enzyme buffer (10×)	2.5 µl	1×
Sucrose (15% (wt/vol))/Orange G (0.05% (wt/vol))	5 µl	3%/0.01%
Restriction enzyme (8–20 U $µl^{-1}$)	0.5 µl	4–10 U
ddH_2O	7 µl	

(ii) Add 15 µl of digestion mixture to the PCR product from Step 3 and mix it by pipetting several times. Incubate the mixture at 37 °C for >2 h.

(iii) Run a 10-µl aliquot of the digestion mixture on a 2% (wt/vol) SYNERGEL + 0.7% (wt/vol) agarose gel in Tris-borate-EDTA buffer. We use the Electro-Fast Gel System for electrophoresis. A loading buffer is not required and the reaction mixture can be directly loaded.

? TROUBLESHOOTING

(B) SNP typing by direct sequencing

(i) Add 20 µl of 1.5× DNA loading buffer to the PCR product.

(ii) Run a 5-µl aliquot of the PCR mixture together with a DNA ladder on a 1.5% (wt/vol) agarose gel to verify amplification of a single genomic fragment of expected size. We detect the band by ethidium bromide staining and UV illumination.

? TROUBLESHOOTING

(iii) Precipitate DNA by adding 3 µl of 3 M sodium acetate (pH 5.2) and 100 µl of 100% (vol/vol) ethanol to the remaining 25 µl of PCR mixture transferred to a 1.5-ml tube.

(iv) Centrifuge the tubes at maximum speed for 10 min, rinse and dry the precipitate.

(v) Dissolve the precipitate in 30 µl of TE and sequence with either of the SNP-typing primers.

74| Analyze SNPs of individual worms by either restriction fragment length polymorphism analysis or direct sequencing of PCR-amplified genomic fragments as described in **Box 2.**
? TROUBLESHOOTING

75| Amplify genomic fragments from candidate loci and sequence them to search for mutations. In most cases, mutations are found in exonic regions or splice sites. EMS treatment predominantly causes GC-AT transitions. Deletion of a short stretch of sequence also occurs at a lower frequency.

TABLE 7 | SNPs for mapping genes to chromosomes.

Chromosome	Allele	Primers	Restriction enzyme
I	*pkP1101*	5′-CGCGTTTCGTAATGTATCG-3′	*Eco*RI
		5′-GAACTTCCAGGTCACTCTGG-3′	
I	*pkP1119*	5′-CTCCATTTTGGAACTCCCAG-3′	*Eco*RI
		5′-TCAAATTTGGCACGTCATCAG-3′	
II	*pkP2107*	5′-TCCACACTATTTCCCTCGTG-3′	*Dra*I
		5′-GAGCAATCAAGAACCGGATC-3′	
III	*pkP3093*	5′-CGCTGAAATTGAGGAGCAG-3′	*Ava*II
		5′-TGGGCTTAACAATGATGGG-3′	
III	*pkP3102*	5′-CATTAGGAAGTGATGCAAGTGG-3′	*Ava*II
		5′-TGGATTTGAGAGGTGTCCATAG-3′	
IV	*pkP4071*	5′-CCAAACAACCTACAGAAAATGC-3′	*Dra*I
		5′-AAGATATTCATGCGTCGTAGTG-3′	
V	*pkP5076*	5′-CGGAAAATTGCGACTGTC-3′	*Dra*I
		5′-ATTAGGACTGCTTGGCTTCC-3′	
V	*pkP5097*	5′-TAGTGTTCATAGCATCCCATTG-3′	*Dra*I
		5′-GTGCTAATTCCAGAAATGATCC-3′	

● TIMING
Steps 1–16, Cloning genomic DNA fragment cassettes into entry vectors: 2–3 weeks
Step 17, Modification of genomic DNA fragment cassettes (optional): 2–3 weeks
Step 18(A), Constructing destination vectors by inverse attB-PCR and BP cloning: 2–3 weeks
Step 18(B), Constructing destination vectors by ligating a promoter fragment to pDEST-PL vector: 2–3 weeks
Steps 19–24, Constructing expression clones: 1–2 weeks
Steps 25–31, Generation of transgenic worms: 3–4 weeks
Steps 32–43, Checking splicing patterns of minigene-derived mRNAs: 2–3 weeks
Steps 44 and 45, Observation of cell type–specific alternative splicing patterns: 2 d
Steps 46–53, Integration of the extrachromosomal array: 3–4 weeks (outcrossing the integrated line will take an additional 3–4 d per generation)
Steps 54–63, Mutant screening: 3–4 weeks (outcrossing the mutant line will take an additional 3–7 d per generation)
Steps 64–75, SNP mapping and mutation search: 2–4 months
Box 1, testing antibiotic resistance: 1–2 d
Box 2, SNP typing: 1–2 d

? TROUBLESHOOTING
Troubleshooting advice can be found in **Table 8.**

TABLE 8 | Troubleshooting table.

Step	Problem	Possible reason	Solution
12, 18A(xiii)	Few or no colonies obtained from BP reaction	Inappropriate primers	Make sure that each *att*B-flanked PCR primer is properly designed or selected
		Inappropriate host strains	Use DB3.1 or *ccd*B Survival competent cells in constructing destination vectors
21	Few or no colonies obtained from LR II Plus reaction	Poor purity of plasmid DNAs	Purify miniprep plasmid DNAs with a standard DNA purification column
31	Little or no expression of fluorescent proteins	Low expression levels	If you obtain many marker-positive and non-fluorescent transgenic lines, check mRNA expression levels as described in Steps 32–43. If mRNA is not detected, try other promoters to drive the minigenes

(continued)

TABLE 8 | Troubleshooting table (continued).

Step	Problem	Possible reason	Solution
		mRNAs are degraded by NMD	Check the design of the minigenes, and reconstruct new minigenes
		Aberrant splicing of the minigene-derived mRNAs	Check splicing patterns of the minigene-derived mRNAs as described in Steps 32–43. Genomic fragments inserted in the minigenes usually undergo proper splicing. If aberrant splicing is detected, trim the genomic fragment (Steps 1–16) or remove the cryptic splice sites by site-directed mutagenesis (Step 17)
		Aberrant translation of the minigene-derived mRNAs	Check expression of the fluorescent proteins by western blotting with anti-GFP and/or anti-RFP antibodies. If expected mRNAs but few proteins are detected, optimize the preferred initiation codons and remove unnecessary ATGs out of frame
		Aberrant folding or instability of the fluorescent proteins	N-terminal tags such as GST may improve the expression of the reporter. Repeated trial and error may be required to establish a reporter reflecting the alternative splicing pattern of the endogenous gene
53	No integrant line obtained	Low efficiency in integrant screening	Use extrachromosomal lines with lower transmission rates; it will be easier to distinguish integrated lines from parental lines. Irradiate as many fluorescent worms as possible and isolate as many uniformly fluorescent F_1 worms as possible
63	No mutant lines established	Sterility or lethality of the mutant	If sterile or arrested F_2 worms with apparent color phenotypes are found, try mutagenesis with reporter heterozygotes or extrachromosomal lines. If dead F_2 embryos with apparent color phenotypes are found, alternative splicing regulator of the minigene may be essential for worm development. One may establish weaker alleles in further screening
		Inappropriate screening strategy	If no F_2 worms with aberrant color phenotypes are found, reconsider the screening strategies, e.g., the tissues in which the reporter is expressed or the structures of the reporter minigenes
74	Responsible locus cannot be narrowed down	Inappropriate crossing or ambiguous F_2 phenotypes	Make sure that crossed F_1 progeny is pooled in Step 66. Make sure that single-worm lysates are collected from F_2 hermaphrodites showing the mutant phenotype in Step 68
		The responsible gene may be within a rearranged region	It is important to outcross the integrated reporter lines before mutagenesis. Use other integrated alleles for mutagenesis
		The responsible gene is close to the locus of the integrated reporter	Use other integrated alleles for mutagenesis
BOX 2, Steps 4A(iii) and 4B(ii)	No or little amplification of genomic fragments by PCR	The isolated F_2 worms are too young	Collect single-worm lysates from gravid F_2 hermaphrodites. Mixing of lysates in Step 70 may be insufficient
	Ambiguous pattern of RFLP or sequencing	Contamination of the F_2 hermaphrodites collected in Step 68 with sperm from F_2 males	Pool the F_1 hermaphrodites at L4 stage in Step 66

ANTICIPATED RESULTS

Here we summarize our success rates for each step in minigene construction. In amplifying genomic DNA fragments for cloning the genomic fragment cassettes in entry vectors, most of the fragments were <3 kb and were specifically amplified from N2 genomic DNA (Steps 1–7). These *att*B-PCR products were successfully cloned by BP II reaction (Steps 10–16), although the probability of clones carrying the correct insert varies from 10% to 90%, probably because of a variable amount of coamplified nonspecific PCR products. Sometimes, we found that the genomic DNA sequences of the N2 worms in our laboratory were different from the reference N2 genomic DNA sequences in the GenBank/EMBL/DDBJ databases (accession nos. NC_003279–NC_003284). We reasoned that this was the result of incorrect base calling in the sequencing process of the reference sequence or of spontaneous mutations during the maintenance of the strain, and we used the fragments as they were. Site-directed mutagenesis (Step 17) was achieved with a success rate of 60–80%, although 10–30% of clones

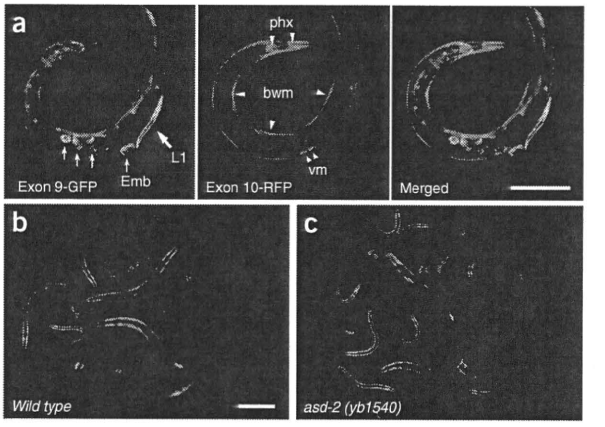

Figure 4 | Visualization of developmental switching of the mutually exclusive exons of the *let-2* gene. The schematic structures of the *let-2* mutually exclusive alternative splicing–reporter minigenes[27] are shown in **Figure 1a**; expression of GFP indicates the selection of embryonic exon 9 and expression of RFP indicates the selection of adult exon 10. (**a**) Confocal images of transgenic worms expressing the *let-2* reporter under the control of a broadly expressing promoter. Left, exon 9–GFP; middle, exon 10–RFP; right, merged view. Note that all tissues in embryos (thin arrows; Emb) and in an L1 larva (large arrow, L1) exclusively express exon 9–GFP, whereas body wall muscles (bwm), pharynx (phx) and vulval muscles (vm) express exon 10–RFP in an adult. Images were acquired with a laser-scanning confocal microscope (Olympus Fluoview 500). (**b**,**c**) Microphotographs of transgenic worms expressing the *let-2* reporter under a body wall muscle-specific promoter in wild-type (**b**) and *asd-2* mutant (**c**) backgrounds. Note that body wall muscles in *asd-2* mutant worms fail to switch from exon 9–GFP to exon 10–RFP during larval development. Images were acquired with an epifluorescence dissecting microscope (Leica MZ16FA) equipped with a dual band-pass filter set (Chroma GFP/DsRed), and a color, cooled CCD camera (Olympus DP71). Scale bars, 100 μm.

contained errors in the oligo DNA sequences. Construction of destination vectors by inverse *att*B-PCR (Step 18A) was less efficient; the rate of correct clones was <10–30%. Therefore, specific amplification of the vector fragment (Step 18A(i)–(iv)) and prescreening by antibiotic resistance (Step 18A(xiii)–(xiv)) are important for higher success probability. Assembling minigenes by LR II Plus reaction (Steps 19–24) was efficient; 60–90% of the carbenicillin-resistant clones in Step 21 carried the correct expression constructs. We did not experience sequence modification in the *att*B homologous recombination sites or in the inserts by LR II Plus reaction.

Construction of fluorescence reporter minigenes (Steps 1–24), generation of transgenic worm lines (Steps 25–31) and imaging of fluorescent reporter worms (Steps 44–45) provides data on the spatiotemporal distribution of alternative splicing events in living worms. We usually use ubiquitous or broadly expressing promoters first to outline expression profiles in *vivo*. In most cases, each tissue expresses either or both fluorescent proteins. In some cases of mutually exclusive alternative splicing reporters, however, expression of fluorescent proteins was not detected in certain tissues, probably because of double-inclusion or double-skipping of alternative exons. We narrow down tissues in which fluorescence reporter minigenes are driven in further genetic analyses as described below.

We recommend confirming that the expression profile of the alternative splicing reporter is consistent with that of the endogenous gene. In case of the *egl-15* gene[26], there was genetic evidence that the *egl-15(5A)* isoform specifically functions in sex myoblasts that differentiate into vulval muscles in hermaphrodites[49]. We confirmed that vulval muscles properly expressed the exon 5A-RFP isoform of the *egl-15* reporter, and the reporter showed muscle specificity when expressed under various tissue-specific promoters[26]. In the case of the *lethal* (*let*)*-2* gene, previous promoter analysis had shown that *let-2* is expressed in body wall muscles and in two distal tip cells[50]. As the number and total mass of body wall muscles are much greater than those of distal tip cells, we reasoned that developmentally regulated switching of *let-2* alternative splicing[51] occurs in body wall muscles. When the *let-2* reporter was expressed under a ubiquitous promoter, all tissues expressed the embryonic form (GFP) in embryos and young larvae, whereas only the body wall muscles turned the reporter expression into the adult form (RFP) during development (**Fig. 4a**), suggesting the presence of tissue-specific and developmental regulation in this event. By using a promoter specific to body wall muscle, we successfully visualized the developmental switching, as shown in the previous study[27] and in **Figure 4b**. In cases of alternative splicing events in which spatiotemporal distributions are unknown, expression profiles of the fluorescence splicing reporter can be confirmed when mutants isolated by phenotype in reporter expression also show the same defect in the splicing pattern of the endogenous gene.

In the screening for mutants defective in the muscle-specific expression of the *egl-15* reporter, we examined the color of the body wall muscles[26], although expression of the endogenous *egl-15* gene was hardly detected in the body wall muscles[52]. We pooled about 300 P_0 worms in total in two independent screenings using two independent integrated alleles. We isolated 15 *alternative splicing defective* (*asd*)*-1* and 10 *suppressor* (*sup*)*-12* alleles[26,28]. The number of *asd-1* alleles was more than expected, and we reasoned that *asd-1*–null mutants are viable and that the ASD-1 coding region has many CAA and CAG codons encoding glutamine, which turn into nonsense TAA and TAG codons after EMS treatment[26]. Although *sup-12*–null mutants are sterile in the *egl-15* reporter homozygous background, we successfully established *sup-12* alleles in the reporter-heterozygous background[28]. Various missense mutations in the RNA-binding domain of SUP-12 caused weaker color phenotypes, suggesting the involvement of these residues in RNA binding[28]. ASD-1 and SUP-12, isolated as regulators in body wall muscles, turned out to be involved in the regulation of the endogenous *egl-15* gene in vulval muscles[26,28].

In the screening for mutants of the *let-2* reporter expression, we mutagenized an integrated allele expressing the *let-2* reporter only in body wall muscles. We used an epifluorescence dissection microscope (MZ16FA) and a dual band-pass filter set and successfully isolated six *asd-2* mutant alleles, all of which continued to express the embryonic form (GFP) in

adulthood (**Fig. 4c**). While searching for *cis*-elements involved in ASD-2-mediated regulation, we disrupted CTAAC repeats in intron 10 of the pair of *let-2* reporter minigenes, as the repeats almost matched the bipartite consensus sequence for QKI[53], a mammalian homolog of ASD-2. The mutant *let-2* reporter showed the same phenotype as *asd-2* mutants, and recombinant ASD-2 protein specifically bound to the CUAAC repeats *in vitro*[27]. Furthermore, the mutant *let-2* reporter no longer responded to overexpression of ASD-2, confirming that ASD-2 functions by binding to CUAAC repeats[27].

Despite our accumulating experience, about half of the fluorescence alternative splicing reporters we generated showed little or no fluorescence. In most of them, the alternative exons themselves encoded hydrophobic stretches; this property may have caused an aggregation or affected folding of the fluorescent proteins. For the rest, transcripts from the reporter were not detected, for which we cannot specify a reason. We therefore focused on the reporters that worked well.

Note: Supplementary information is available via the HTML version of this article.

ACKNOWLEDGMENTS We thank A. Fire, H.R. Horvitz, R.Y. Tsien and A. Miyawaki for materials. We thank the present and past members of Masatoshi Hagiwara lab for their suggestions. We thank M. Hagiwara, H. Ito, Y. Kikuchi, T. Yamada and K. Kawamata for technical assistance. We thank *Caenorhabditis* Genetics Center for strains. We acknowledge support from grants from the Ministry of Education, Culture, Sports, Science and Technology (MEXT), the Japan Society for the Promotion of Science and the Japan Science and Technology Agency (JST).

AUTHOR CONTRIBUTIONS H.K. designed and performed the experiments, and wrote the paper; G.O., H.S. and H.M. designed and performed the experiments to improve the procedure; M.H. organized the study.

COMPETING FINANCIAL INTERESTS The authors declare no competing financial interests.

Published online at http://www.natureprotocols.com/.
Reprints and permissions information is available online at http://npg.nature.com/reprintsandpermissions/.

1. Wang, E.T. *et al.* Alternative isoform regulation in human tissue transcriptomes. *Nature* **456**, 470–476 (2008).
2. Matlin, A.J., Clark, F. & Smith, C.W. Understanding alternative splicing: towards a cellular code. *Nat. Rev. Mol. Cell. Biol.* **6**, 386–398 (2005).
3. Black, D.L. Mechanisms of alternative pre-messenger RNA splicing. *Annu. Rev. Biochem.* **72**, 291–336 (2003).
4. Jin, Y. *et al.* A vertebrate RNA-binding protein Fox-1 regulates tissue-specific splicing via the pentanucleotide GCAUG. *EMBO J.* **22**, 905–912 (2003).
5. Jensen, K.B. *et al.* Nova-1 regulates neuron-specific alternative splicing and is essential for neuronal viability. *Neuron* **25**, 359–371 (2000).
6. Ladd, A.N., Charlet, N. & Cooper, T.A. The CELF family of RNA binding proteins is implicated in cell-specific and developmentally regulated alternative splicing. *Mol. Cell. Biol.* **21**, 1285–1296 (2001).
7. Sheives, P. & Lynch, K.W. Identification of cells deficient in signaling-induced alternative splicing by use of somatic cell genetics. *RNA* **8**, 1473–1481 (2002).
8. Wang, Z., Rolish, M.E., Yeo, G., Tung, V., Mawson, M. & Burge, C.B. Systematic identification and analysis of exonic splicing silencers. *Cell* **119**, 831–845 (2004).
9. Ellis, P.D., Smith, C.W. & Kemp, P. Regulated tissue-specific alternative splicing of enhanced green fluorescent protein transgenes conferred by alpha-tropomyosin regulatory elements in transgenic mice. *J. Biol. Chem.* **279**, 36660–36669 (2004).
10. Oltean, S. *et al.* Alternative inclusion of fibroblast growth factor receptor 2 exon IIIc in Dunning prostate tumors reveals unexpected epithelial mesenchymal plasticity. *Proc. Natl. Acad. Sci. USA* **103**, 14116–14121 (2006).
11. Levinson, N. *et al.* Use of transcriptional synergy to augment sensitivity of a splicing reporter assay. *RNA* **12**, 925–930 (2006).
12. MacMorris, M.A., Zorio, D.A. & Blumenthal, T. An exon that prevents transport of a mature mRNA. *Proc. Natl. Acad. Sci. USA* **96**, 3813–3818 (1999).
13. Newman, E.A. *et al.* Identification of RNA-binding proteins that regulate FGFR2 splicing through the use of sensitive and specific dual color fluorescence minigene assays. *RNA* **12**, 1129–1141 (2006).
14. Orengo, J.P., Bundman, D. & Cooper, T.A. A bichromatic fluorescent reporter for cell-based screens of alternative splicing. *Nucleic Acids Res.* **34**, e148 (2006).
15. Warzecha, C.C., Sato, T.K., Nabet, B., Hogenesch, J.B. & Carstens, R.P. ESRP1 and ESRP2 are epithelial cell-type-specific regulators of FGFR2 splicing. *Mol. Cell* **33**, 591–601 (2009).
16. Oltean, S., Febbo, P.G. & Garcia-Blanco, M.A. Dunning rat prostate adenocarcinomas and alternative splicing reporters: powerful tools to study epithelial plasticity in prostate tumors *in vivo*. *Clin. Exp. Metastasis* **25**, 611–619 (2008).
17. Stoilov, P., Lin, C.H., Damoiseaux, R., Nikolic, J. & Black, D.L. A high-throughput screening strategy identifies cardiotonic steroids as alternative splicing modulators. *Proc. Natl. Acad. Sci. USA* **105**, 11218–11223 (2008).
18. Bonano, V.I., Oltean, S. & Garcia-Blanco, M.A. A protocol for imaging alternative splicing regulation *in vivo* using fluorescence reporters in transgenic mice. *Nat. Protoc.* **2**, 2166–2181 (2007).
19. Bonano, V.I., Oltean, S., Brazas, R.M. & Garcia-Blanco, M.A. Imaging the alternative silencing of *FGFR2* exon IIIb *in vivo*. *RNA* **12**, 2073–2079 (2006).
20. Takeuchi, A., Hosokawa, M., Nojima, T. & Hagiwara, M. Splicing reporter mice revealed the evolutionally conserved switching mechanism of tissue-specific alternative exon selection. *PLoS One* **5**, e10946 (2010).
21. Zahler, A.M. Alternative splicing in *C. elegans*. in *WormBook* (ed. The *C. elegans* Research Community). doi:10.1895/wormbook.1.31.1, http://www.wormbook.org (26 September 2005).
22. Spike, C.A., Davies, A.G., Shaw, J.E. & Herman, R.K. MEC-8 regulates alternative splicing of *unc-52* transcripts in *C. elegans* hypodermal cells. *Development* **129**, 4999–5008 (2002).
23. Spartz, A.K., Herman, R.K. & Shaw, J.E. SMU-2 and SMU-1, *Caenorhabditis elegans* homologs of mammalian spliceosome-associated proteins RED and fSAP57, work together to affect splice site choice. *Mol. Cell. Biol.* **24**, 6811–6823 (2004).
24. Spike, C.A., Shaw, J.E. & Herman, R.K. Analysis of *smu-1*, a gene that regulates the alternative splicing of *unc-52* pre-mRNA in *Caenorhabditis elegans*. *Mol. Cell. Biol.* **21**, 4985–4995 (2001).
25. Kabat, J.L., Barberan-Soler, S., McKenna, P., Clawson, H., Farrer, T. & Zahler, A.M. Intronic alternative splicing regulators identified by comparative genomics in nematodes. *PLoS Comput. Biol.* **2**, e86 (2006).
26. Kuroyanagi, H., Kobayashi, T., Mitani, S. & Hagiwara, M. Transgenic alternative-splicing reporters reveal tissue-specific expression profiles and regulation mechanisms *in vivo*. *Nat. Methods* **3**, 909–915 (2006).
27. Ohno, G., Hagiwara, M. & Kuroyanagi, H. STAR family RNA-binding protein ASD-2 regulates developmental switching of mutually exclusive alternative splicing *in vivo*. *Genes Dev.* **22**, 360–374 (2008).
28. Kuroyanagi, H., Ohno, G., Mitani, S. & Hagiwara, M. The Fox-1 family and SUP-12 coordinately regulate tissue-specific alternative splicing *in vivo*. *Mol. Cell. Biol.* **27**, 8612–8621 (2007).
29. Lander, E.S. *et al.* Initial sequencing and analysis of the human genome. *Nature* **409**, 860–921 (2001).
30. David, C.J. & Manley, J.L. The search for alternative splicing regulators: new approaches offer a path to a splicing code. *Genes Dev.* **22**, 279–285 (2008).
31. Kuroyanagi, H. Fox-1 family of RNA-binding proteins. *Cell. Mol. Life Sci.* **66**, 3895–3907 (2009).
32. Mello, C.C., Kramer, J.M., Stinchcomb, D. & Ambros, V. Efficient gene transfer in *C.elegans*: extrachromosomal maintenance and integration of transforming sequences. *EMBO J.* **10**, 3959–3970 (1991).
33. Van Buskirk, C. & Sternberg, P.W. Epidermal growth factor signaling induces behavioral quiescence in *Caenorhabditis elegans*. *Nat. Neurosci.* **10**, 1300–1307 (2007).
34. Chang, Y.F., Imam, J.S. & Wilkinson, M.F. The nonsense-mediated decay RNA surveillance pathway. *Annu. Rev. Biochem.* **76**, 51–74 (2007).

35. Isken, O. & Maquat, L.E. Quality control of eukaryotic mRNA: safeguarding cells from abnormal mRNA function. *Genes Dev.* **21**, 1833–1856 (2007).
36. Pulak, R. & Anderson, P. mRNA surveillance by the *Caenorhabditis elegans smg* genes. *Genes Dev.* **7**, 1885–1897 (1993).
37. Burgess, R.R. Use of bioinformatics in planning a protein purification. *Methods Enzymol.* **463**, 21–28 (2009).
38. Brondyk, W.H. Selecting an appropriate method for expressing a recombinant protein. *Methods Enzymol.* **463**, 131–147 (2009).
39. Mello, C.C. & Fire, A. DNA transformation. in *Caenorhabditis elegans: Modern Biological Analysis of an Organism* (eds. Epstein, H.F. & Shakes, D.C.) 452–482 (Academic Press, San Diego, 1995).
40. Clark, S.G., Lu, X. & Horvitz, H.R. The *Caenorhabditis elegans* locus *lin-15*, a negative regulator of a tyrosine kinase signaling pathway, encodes two different proteins. *Genetics* **137**, 987–997 (1994).
41. Mitani, S. Genetic regulation of *mec-3* gene expression implicated in the specification of the mechanosensory neuron cell types in *Caenorhabditis elegans*. *Dev. Growth Differ.* **37**, 551–557 (1995).
42. Caceres, J.F. & Kornblihtt, A.R. Alternative splicing: multiple control mechanisms and involvement in human disease. *Trends Genet.* **18**, 186–193 (2002).
43. Wicks, S.R., Yeh, R.T., Gish, W.R., Waterston, R.H. & Plasterk, R.H. Rapid gene mapping in *Caenorhabditis elegans* using a high density polymorphism map. *Nat. Genet.* **28**, 160–164 (2001).
44. Ryder, S.P., Recht, M.I. & Williamson, J.R. Quantitative analysis of protein-RNA interactions by gel mobility shift. *Methods Mol. Biol.* 99–115 (2008).
45. Clarke, P.A. Labeling and purification of RNA synthesized by *in vitro* transcription. in *RNA-Protein Interaction Protocols* (ed. Haynes, S.R.) 1–10 (Humana Press, Totowa, New Jersey, 1999).
46. Ohno, M. & Shimura, Y. Nuclear cap binding protein from HeLa cells. *Methods Enzymol.* **181**, 209–215 (1990).
47. Johnstone, I.L. Molecular biology. in *C. elegans: A Practical Approach* (ed. Hope, I.A.) 201–225 (Oxford University Press, New York, 1999).
48. Inoue, H., Nojima, H. & Okayama, H. High efficiency transformation of *Escherichia coli* with plasmids. *Gene* **96**, 23–28 (1990).
49. Goodman, S.J., Branda, C.S., Robinson, M.K., Burdine, R.D. & Stern, M.J. Alternative splicing affecting a novel domain in the *C. elegans* EGL-15 FGF receptor confers functional specificity. *Development* **130**, 3757–3766 (2003).
50. Graham, P.L., Johnson, J.J., Wang, S., Sibley, M.H., Gupta, M.C. & Kramer, J.M. Type IV collagen is detectable in most, but not all, basement membranes of *Caenorhabditis elegans* and assembles on tissues that do not express it. *J. Cell. Biol.* **137**, 1171–1183 (1997).
51. Sibley, M.H., Johnson, J.J., Mello, C.C. & Kramer, J.M. Genetic identification, sequence, and alternative splicing of the *Caenorhabditis elegans* alpha 2(IV) collagen gen. *J. Cell. Biol.* **123**, 255–264 (1993).
52. Kostas, S.A. & Fire, A. The T-box factor MLS-1 acts as a molecular switch during specification of nonstriated muscle in *C. elegans*. *Genes Dev.* **16**, 257–269 (2002).
53. Galarneau, A. & Richard, S. Target RNA motif and target mRNAs of the Quaking STAR protein. *Nat. Struct. Mol. Biol.* **12**, 691–698 (2005).

⌘ *Author's Choice*

THE JOURNAL OF BIOLOGICAL CHEMISTRY VOL. 285, NO. 8, pp. 5532–5540, February 19, 2010

Regulation of Vascular Endothelial Growth Factor (VEGF) Splicing from Pro-angiogenic to Anti-angiogenic Isoforms

*A NOVEL THERAPEUTIC STRATEGY FOR ANGIOGENESIS**

Received for publication, October 13, 2009 Published, JBC Papers in Press, November 11, 2009, DOI 10.1074/jbc.M109.074930

Dawid G. Nowak[‡1], Elianna Mohamed Amin[§1], Emma S. Rennel[‡], Coralie Hoareau-Aveilla[‡], Melissa Gammons[‡], Gopinath Damodoran[‡], Masatoshi Hagiwara[¶], Steven J. Harper[‡], Jeanette Woolard[‡2], Michael R. Ladomery[§2,3], and David O. Bates[‡2,4]

From the [‡]Microvascular Research Laboratories, Bristol Heart Institute, Department of Physiology and Pharmacology, School of Veterinary Sciences, University of Bristol, Bristol BS2 8EJ, United Kingdom, the [§]Centre for Research in Biomedicine, School of Life Sciences, University of the West of England, Bristol BS16 1QY, United Kingdom, and the [¶]Department of Genetics, University of Tokyo Medical and Dental School, Tokyo 113-8510, Japan

Vascular endothelial growth factor (VEGF) is produced either as a pro-angiogenic or anti-angiogenic protein depending upon splice site choice in the terminal, eighth exon. Proximal splice site selection (PSS) in exon 8 generates pro-angiogenic isoforms such as $VEGF_{165}$, and distal splice site selection (DSS) results in anti-angiogenic isoforms such as $VEGF_{165}b$. Cellular decisions on splice site selection depend upon the activity of RNA-binding splice factors, such as ASF/SF2, which have previously been shown to regulate VEGF splice site choice. To determine the mechanism by which the pro-angiogenic splice site choice is mediated, we investigated the effect of inhibition of ASF/SF2 phosphorylation by SR protein kinases (SRPK1/2) on splice site choice in epithelial cells and in *in vivo* angiogenesis models. Epithelial cells treated with insulin-like growth factor-1 (IGF-1) increased PSS and produced more $VEGF_{165}$ and less $VEGF_{165}b$. This down-regulation of DSS and increased PSS was blocked by protein kinase C inhibition and SRPK1/2 inhibition. IGF-1 treatment resulted in nuclear localization of ASF/SF2, which was blocked by SPRK1/2 inhibition. Pull-down assay and RNA immunoprecipitation using VEGF mRNA sequences identified an 11-nucleotide sequence required for ASF/SF2 binding. Injection of an SRPK1/2 inhibitor reduced angiogenesis in a mouse model of retinal neovascularization, suggesting that regulation of alternative splicing could be a potential therapeutic strategy in angiogenic pathologies.

Vascular endothelial growth factor (VEGF-A, hereafter referred to as VEGF)[5] is a key regulatory component in physiological and pathological angiogenesis. Inhibition of VEGF has shown to be effective in cancer (1) and ocular angiogenesis (2), and it is up-regulated by a number of growth factors also implicated in these conditions, including insulin-like growth factor-1 (IGF-1) (3). VEGF is generated as multiple isoforms by alternative splicing (4). There are two principal families of VEGF isoforms, the pro-angiogenic $VEGF_{xxx}$ isoforms, generated by proximal splice site selection in the terminal exon, exon 8a (5), and the anti-angiogenic $VEGF_{xxx}b$ isoforms (6), generated by use of a distal splice site 66 bp further into exon 8, generating mRNA isoforms that contain exon 8b. As the stop codon for the protein is encoded in exon 8, these two isoforms contain alternate six amino acids at the C terminus (Fig. 1*A*). The pro-angiogenic isoforms such as $VEGF_{165}$ encode a terminal six amino acid sequence of CDKPRR, and the anti-angiogenic isoforms such as $VEGF_{165}b$ encode SLTRKD (7). Many normal tissues, including the eye generate both isoforms (8), and previous studies have shown that the anti-angiogenic isoforms dominate in non-angiogenic tissues such as the normal colon (9) and the vitreous (8). However, there is a splicing switch in angiogenic conditions such as proliferative diabetic retinopathy (8), colon (9), prostate (10), renal (7), and skin cancers (11), and in Denys Drash Syndrome (12). In contrast, in non-angiogenic conditions where VEGF is up-regulated, such as glaucoma and rhegmatogenous retinal detachment associated with proliferative vitreoretinopathy (13) or glaucoma (14), the anti-angiogenic isoforms are up-regulated. We have previously shown that IGF-1 can switch splicing in cultured epithelial cells from anti-angiogenic to pro-angiogenic isoforms (15). As IGF-1 has been implicated in a number of angiogenic conditions including diabetic retinopathy and colon cancer, we hypothesized that the mechanism through which IGF-1 mediates this change in splicing may be a potential therapeutic target to prevent angiogenesis. To this end, we have investigated the signaling pathways, the splicing factors involved, and the possibility of therapeutic intervention in the pathway in an animal model of diabetic retinopathy.

* This work was supported by the British Heart Foundation (FS/04/09 and BS/06/005), the Wellcome Trust (79633), a University of West of England Bristol PhD Studentship, the Richard Bright VEGF Research Trust, Fight for Sight, Cancer Research UK (C11392/A10484), and the Skin Cancer Research Fund.

⌘ *Author's Choice*—Final version full access.

[1] Both authors contributed equally to this work.

[2] Joint senior authors.

[3] To whom correspondence may be addressed. E-mail: Michael.Ladomery@uwe.ac.uk.

[4] To whom correspondence may be addressed. E-mail: Dave.Bates@bris.ac.uk.

[5] The abbreviations used are: VEGF, vascular endothelial growth factor; IGF-1, insulin-like growth factor; nt, nucleotide; PBS, phosphate-buffered saline; PKC, protein kinase C; ELISA, enzyme-linked immunosorbent assay; MBP, maltose-binding protein; PSS, proximal splice site selection; OIR, oxygen-induced retinopathy; UTR, untranslated region; ITS, insulin transferrin selenium; PMA, phorbol myristate acetate; HEK, human embryonic kidney.

TABLE 1
Primer sequences

Construct A	Forward:5′-GAATTCCTCATCGCCAGGCCTCCTCACTTG-3′
	Reverse:5′-GGATTCCCTTCGCCGGAGTCTCGCCCTC-3′
Construct B	Forward:5′-GAATTCCGCCCTAACCCCAGCCTTTGTTTTCCATTTCCC-3′
	Reverse:5′-GGATCCGGACTGTTCTGTCGATGGTG-3′
Construct C	Forward:5′-GAATTCCGCCCTAACCCCAGCCTTTGTTTTCCATTTCCC-3′
	Reverse:5′-GGATCCTGGTTCCCGAAACCCTGAGCG-3′
Construct D	Forward:5′-GATTCCGAGGAAGGAAGGAGCCTCCCTCAGGG-3′
	Reverse:5′-GGATCCGGACTGTTCTGTCGATGGTG-3′
Construct E	Forward:5′-GAATTCATGTGACAAGCCGAGGCGG-3′
	Reverse:5′-GGATCCCTGGTTCCCGAAACCCTGAGCG-3′
Mouse VEGF-A ex 7 F	Forward 5′ GTTCAGAGCGGAGAAAGCAT-3′
Mouse VEGF-A ex 8a R	Reverse 5′TCACATCTGCAAGTACGTTCG-3′
Mouse VEGF-A ex 2 F	Forward 5′ AAGGAGAGCAGAAGTCCCATGA-3′
Mouse VEGF-A ex 3 R	Reverse 5′ CTCAATCGGACGGCAGTAGCT-3′
β-Actin F	Forward 5′ AGCCATGTACGTAGCCATCC-3′
β-Actin R	Reverse 5′ CTCTCAGCTGTGGTGGTGAA-3′

EXPERIMENTAL PROCEDURES

Proliferating Podocytes—PCIPs (courtesy of Moin Saleem, University of Bristol, Bristol, UK) were derived from a cell line conditionally transformed from normal human podocytes with a temperature-sensitive mutant of immortalized SV-40 T-antigen. At the permissive temperature of 33 °C, the SV-40 T-antigen is active and allows the cells to proliferate rapidly (16). PCIPs were cultured in T75 flasks (Greiner) in RPMI 1640 medium (Sigma) with 10% fetal bovine serum, 1% ITS (insulin transferrin selenium) (Sigma), 0.5% penicillin-streptomycin solution (Sigma), and grown to 95% confluency. Then cells were split into 6-well plates (2×10^5 cells per well) and grown until 95% confluency.

Treatments with IGF-1 and Pharmacological Inhibitors—To investigate the inhibitory effect of IGF-1 on $VEGF_{xxx}b$ mRNA and protein synthesis, pharmacological inhibitors and IGF-1 with PKC-BIMI (Calbiochem), and SRPK1/2 (SR protein kinases 1 and 2)-SRPIN340 (SR protein phosphorylation inhibitor 340) (17) were used. 24 h before treatment, cultured medium was replaced with serum-free RPMI 1640 medium (Sigma) containing 1% ITS (Sigma) and 0.5% penicillin-streptomycin (Sigma). Subsequently, the medium was replaced with fresh serum-free RPMI 1640 medium (Sigma) containing 1% ITS, 0.5% penicillin-streptomycin, and either 2.5 μM BIMI (bisindolylmaleimide 1) or 10 μM SRPIN340 for 60 min before treatment with IGF-1. 12 h after stimulation, RNA was extracted, and 48 h after stimulation, proteins were extracted.

RT-PCR—1 μg of mRNA was reverse transcribed using MMLV RT, RNase H Minus, point mutant (Promega), and oligo$(dT)_{15}$ (Promega) as a primer. The reaction was carried out in Bio-Rad cycler for 60 min at 40 °C, and then the enzyme was inactivated at 70 °C for 15 min. Ten percent of the cDNA was then amplified using primers designed to pick up proximal and distal splice forms. 1 μM of each primer (exon 7b 5′-GGCAGCTTGAGTTAAACGAAC-3′, exon 8b 5′-ATGGATCCGTATCAGTCTTTCCTGG-3′) and PCR Master Mix (Promega) were used in reactions cycled 30 times, denaturing at 95 °C for 60 s, annealing at 55 °C for 60 s, and extending at 72 °C for 60 s. PCR products were run on 2.5% agarose gels containing 0.5 μg/ml ethidium bromide and visualized under a UV transilluminator. This reaction usually resulted in one amplicon of 130 bp ($VEGF_{xxx}$) and one amplicon of 64 bp ($VEGF_{xxx}b$). For HEK293 and HeLa cells, RT-PCR was performed using primers specific to exon 7a and the 3′-untranslated region of the VEGF mRNA. The primers used were 5′-GTAAGCTTGTACAAGATCCGCAGACG-3′ and 5′-ATGGATCCGTATCAGTCTTTCCTGG-3′. The reaction was set up in a 20-μl reaction using the 2× FastStart Universal SyBR Master Mix (Roche, cat. no: 04913850001) and 1 μM each primer. The reaction was performed on the ABI 7000 cycler for 95 °C for 10 min, followed by 30 cycles of 95 °C for 15 s and 55 °C for 30 s.

Western Blotting—Protein samples were dissolved in Laemmli buffer, boiled for 3–4 min, and centrifuged for 2 min at 20,000 × *g* to remove insoluble materials. 30 μg of protein per lane were separated by SDS/PAGE (12%) and transferred to a 0.2-μm nitrocellulose membrane. The blocked membranes were probed overnight (4 °C) with antibodies against panVEGF (R&D; MAB 293, 1:500), $VEGF_{xxx}b$ (R&D Systems; MAB3045; 1:250), ASF/SF2 antibody (Santa Cruz Biotechnology; sc-10254; 1:1000), and β-tubulin (Sigma, 1:2000). Western blotting has previously shown that all the proteins recognized by the $VEGF_{xxx}b$ antibody are also recognized by commercial antibodies raised against $VEGF_{165}$. It binds recombinant $VEGF_{165}b$, and can be used to demonstrate expression of $VEGF_{165}b$, $VEGF_{189}b$, and $VEGF_{121}b$ (collectively termed $VEGF_{xxx}b$) but does not recognize $VEGF_{165}$, conclusively demonstrating that this antibody is specific for $VEGF_{xxx}b$ (6). Subsequently, the membranes were incubated with secondary horseradish peroxidase-conjugated antibody, and immunoreactive bands were visualized using ECL reagent (Pierce). Immunoreactive bands corresponding to panVEGF and $VEGF_{xxx}b$ in each treatment were quantified by ImageJ analysis and normalized to those of β-tubulin or β-actin. Blots are representative of at least three experiments. Densitometry was carried out by scanning in gels and using ImageJ to determine gray levels of bands and background.

Construction of Plasmids—The VEGF sequence of interest (from 35-bp upstream of exon 8a to 35-bp downstream of exon 8b) was amplified from a BAC DNA template using 50 ng of BAC DNA, 10 μM of each primers (see Table 1), 10 mM dNTP mix (Promega), and Taq polymerase (Promega). A modified ADML-MS2 plasmid was digested with EcoR1 and BamH1, and PCR products ligated into the vector and subsequently transformed. Colonies were selected, and plasmid extraction (Qiagen) was performed. The identities of the plasmids were confirmed by sequencing.

Expression of the MS2-MBP (Maltose-binding Protein) Fusion Protein—MS2-MBP (a gift from Robin Reed, Harvard University) was expressed in *Escherichia coli* DH5α. The cells were grown to an optical density of ~0.5 at 600 nm and induced for expression for 3 h with 0.2 mM isopropyl-1-thio-β-D-galactopyranoside. The MS2-MBP protein was purified by amylose beads according to the manufacturer's protocol (NEB, Beverly, MA). The protein was dialyzed with 10 mM sodium phosphate, pH 7, overnight at 4 °C, to remove existing salts that are present and further purified over a Heparin Hi Trap column using a NaCl gradient (GE Healthcare). An immunoblot analysis was performed on the purified fusion proteins using rabbit anti-MS2 antibody (gift from Peter Stockley, Leeds University) to confirm the identity of the protein.

Assembly of the MS2-MBP System—1 μg of the VEGF-MS2 plasmid was linearized with XbaI and in *vitro* transcribed with T7 RNA polymerase (NEB) in 0.5 mM rNTP (Ambion), 40 mM Tris-HCl, 6 mM $MgCl_2$, 10 mM dithiothreitol, 2 mM spermidine at 40 °C for 1 h to make VEGF-MS2 RNA. A 100-fold molar excess of MS2-MBP fusion protein and VEGF-MS2 RNA were incubated in a buffer containing 20 mM HEPES, pH 7.9 and 60 mM NaCl on ice for 30 min. 75 mg of HEK293 nuclear extract were added to the MS2-MBP fusion protein/VEGF-RNA mix in 0.5 mM ATP, 6.4 mM $MgCl_2$, 20 mM creatine phosphate for 1 h at 30 °C. Proteins that bound to the MS2-MBP/VEGF-MS2 RNA complex were affinity selected on amylose beads by rotating for 4 h at 4 °C and eluted with 12 mM maltose, 20 mM HEPES pH 7.9, 60 mM NaCl, 10 mM β-mercaptoethanol, and 1 mM phenylmethylsulfonyl fluoride.

RNA Immunoprecipitation—HEK293 cells were transfected with plasmid containing the last 131 nt of intron 7 and the first 152 nt of exon 8 inserted downstream of the CMV promoter in pTARGET. Two variants of this were generated by site-directed mutagenesis: a deletion of 11 nucleotides upstream of the PSS from −4 to −24 nt, and the second is a mutation of the sequence CTTTGTTTTCCATTTC to GGGGGGGGGGCAGGGG. Cells were cross-linked for 10 min at 4 °C with 1% formaldehyde in phosphate-buffered saline and blocked by the addition of glycine, pH 8, at a final concentration of 250 mM. The cells were washed twice with PBS, and the cell pellet resuspended in 500 μl of radioimmune precipitation assay buffer (50 mM, Tris-Cl, pH 7.5, 150 mM NaCl, 1 mM EDTA, 1% Nonidet P-40, 0.5% sodium deoxycholate, 0.05% SDS) and incubated on ice for 20 min. The cells were sonicated three times for 15 s with an XL ultrasonic homogenizer (setting 5) and incubated on ice for 2 min between each sonication. The extract was centrifuged for 10 min at 10,000 rpm and precleared by a 1-h incubation at room temperature with protein A-agarose beads (previously coated with 0.5 mg/ml bovine serum albumin and 0.2 mg/ml herring sperm DNA). The antibodies mouse IgG (vector I-200) or anti-ASF/SF2 (SC96, Santa Cruz Biotechnology) were incubated for 1 h at room temperature with protein A-agarose beads (Sigma, coated as above). ASF/SF2-containing complexes were pulled down after a 2-h incubation of the precleared extract with the antibody/beads and washed six times for 10 min each in 50 mM Tris-Cl, pH 7.5, 1 M NaCl, 1 mM EDTA, 1% Nonidet P-40, 1% sodium deoxycholate, 0.1% SDS, 1.5 M urea. The complexes were eluted and cross-link reversed by treatment for 45 min at 70 °C with 50 mM Tris-Cl, pH 7.5, 5 mM EDTA, 10 mM dithiothreitol, and 1% SDS. RNA was then extracted with Tri-reagent solution (Ambion) according to the manufacturer's protocol, precipitated with 0.8 volumes of isopropyl alcohol in the presence of glycoblue (Ambion), the pellet resuspended in water, and subjected to DNase treatment for 1 h at 37 °C and reverse transcription for 1 h at 42 °C using MMLV (Promega) and oligo$(dT)_{15}$. PCR was carried out using the Master Mix from Promega and specific primers for the plasmid VEGF sequence. 5′-CTAGCCTCGAGACGCGTGAT-3′ and 5′-GGCAGCGTGGTTTCTGTATC-3′ or GAPDH.

Oxygen-induced Retinopathy (OIR)—The OIR model was performed as previously described (18, 19) with minor modifications. Neonatal C57/Bl6 mice and nursing CD1 dams were exposed to 75% oxygen between P7 and P12. Return to room air induced hypoxia in the ischemic areas. On P13, mice received either HBSS or SRPIN340 (10 pmol) in Hank's-buffered solution in a 1-μl intraocular injections using a Nanofil syringe fitted with a 35-gauge needle (WPI, Sarasota, FL) into the left eye under isoflurane anesthesia. On P17, both eyes were dissected, fixed in 4% paraformaldehyde overnight at 4 °C, and retinas were dissected. Retinas were permeabilized in PBS containing 0.5% Triton X-100 and 1% bovine serum albumin, stained with 20 μg/ml biotinylated isolectin B4 (Sigma Aldrich) in PBS, pH 6.8, 1% Triton X-100, 0.1 mM $CaCl_2$, 0.1 mM $MgCl_2$, followed by 20 μg/ml ALEXA 488-streptavidin (Molecular Probes, Eugene, OR) and flat mounted in Vectashield (Vector Laboratories, Burlingame, CA). Retinas were examined under a Nikon Eclipse 400 epifluorescence microscope and areas of neovascularization identified under a 4× objective. Images were captured and imported into Image J, and neovascular, ischemic, and normal areas were traced and measured. Imaging was done by investigator, blinded to treatment.

Real-time PCR on Mouse OIR Retina—HBSS or 100 pmol of SRPIN340 in 1 μl was injected intraocularly into OIR pups on day 13 (day 7–12 in 75% O_2), and after 48 h, the eyes were enucleated and placed in RNAlater (Sigma Aldrich), and the retinae were excised. Total RNA was extracted using RNAeasy (Qiagen) according to the manufacturer's manual, and 0.3 μg of DNase-digested total RNA was reverse transcribed using the oligo(dT_{15}) primer. Real-time PCR was performed on a Cepheid Real time thermocycler using ABsolute QPCR SYBR green mix (Thermo Scientific) and 70 nM primers specific for $VEGF_{165}$ (exon 7/8a) or total VEGF (exon 2/3) at 95 °C for 15 min, then 95 °C for 15 s, and 60 °C for 30 s × 40 cycles or for the housekeeping gene (β-actin) 95 °C 15 min, at 95 °C for 15 s, 55 °C for 30 s, 72 °C for 30 s × 40 cycles.

Immunocytofluorescence—Cells were washed with PBS, fixed for 5 min with 4% (w/v) PFA, washed with PBS in 0.05% Triton X (PBS-T) blocked in 5% horse serum in PBS-T (1 h), washed three times, and incubated overnight with 2 μg/ml of anti-ASF/SF2 (SC10255) or a nonspecific goat IgG, washed, and incubated with donkey anti-goat Alexa Fluor 594 for visualization and counterstained for the nucleus with Hoechst. Images were taken at 40× magnification with the Nikon Eclipse 400 epifluorescence microscope or 60× on a Perkin Elmer Ultraview-Fret H confocal microscopy system.

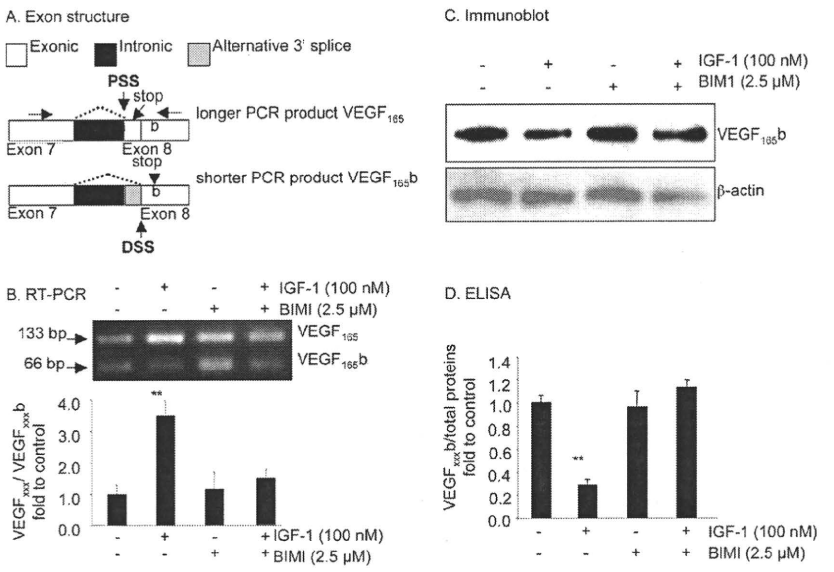

FIGURE 1. **Inhibition of PKC by BIM1 prevents the down-regulation of $VEGF_{xxx}b$ by IGF.** *A*, exon structure of the VEGF pre-mRNA. Alternative splicing of exon 8 to either 8a or 8b results in use of proximal (*PSS*) or distal splice sites (*DSS*) resulting in shorter mRNA for distal splicing. Because the last stop codon is missing, the final six amino acid open reading frame is replaced by an identically sized open reading frame encoding six different amino acids. The primer position is shown by *horizontal arrows*. *B–D*, podocytes were treated with BIM1 (2.5 μM) alone or in combination with IGF-1 (100 nM). *B*, RT-PCR showed that BIM1 reduced the $VEGF_{xxx}$:$VEGF_{xxx}b$ ratio at the RNA level. *C*, Western blot demonstrating that BIM1 inhibited the IGF-mediated down-regulation of $VEGF_{xxx}b$ expression at the protein level. *D*, ELISA results confirming that BIM1 specifically attenuated the IGF-1-dependent down-regulation of $VEGF_{xxx}b$, but does not affect endogenous expression of $VEGF_{xxx}b$. **, $p < 0.01$ compared with untreated.

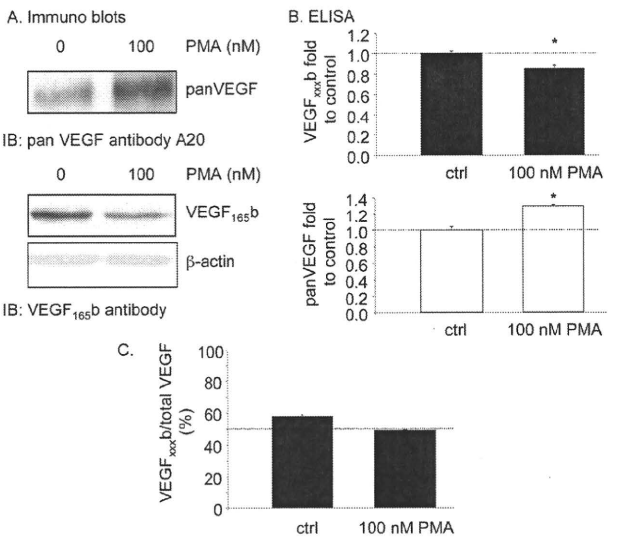

FIGURE 2. **Proximal splicing is activated by protein kinase C.** *A–C*, treatment of podocytes with the PKC activator PMA reduced $VEGF_{165}b$ expression, but increased expression of total VEGF as measured by Western blot (*A*) and ELISA (*B*). This results in a change of relative expression from 60% (anti-angiogenic) to just under 50% (angiogenic) (*C*).

Statistical Analysis—Statistical analyses were carried out on raw data using the Friedman test (Dunnet post-test), and a p value of less than 0.05 was considered statistically significant. Values are expressed as means ± S.E. For all data, n represents the number of independent cell populations or derived from different donors.

RESULTS

The IGF-1-dependent Switch between Isoforms Is PKC-dependent—To determine whether the IGF-1-mediated switch in splicing was regulated by PKC inhibition, podocytes were incubated with pharmacological inhibitors of PKC (BIMI). Treatment with 100 nM IGF-1 and 2.5 μM BIMI, the PKC inhibitor, followed by RNA extraction and RT-PCR using primers that detect both proximal ($VEGF_{xxx}$, 130-bp amplicon) and distal splice isoforms ($VEGF_{xxx}b$, 64 bp amplicon) was carried out. Treatment with IGF-1 increased the relative intensity of the $VEGF_{xxx}$ (upper) band to the $VEGF_{xxx}b$ band (lower) from 1.39 ± 0.42 to 4.84 ± 0.65 ($p < 0.01$, Fig. 1*B*). Treatment with 100 nM IGF-1 and 2.5 μM BIMI, the PKC inhibitor, resulted in a $VEGF_{xxx}$:$VEGF_{xxx}b$ density of 2.12 ± 0.39, which was lower than treatment with IGF-1 alone (4.84 ± 0.65, $p < 0.05$) but was not different from treatment with BIMI alone (1.62 ± 0.76, $p > 0.05$, Fig. 1*B*).

To determine whether IGF-1-mediated regulation of splicing was apparent at the protein level, podocytes were incubated with the pharmacological inhibitors of PKC (BIMI), and ELISA carried out on the protein extracted from the cells. Treatment with 100 nM IGF-1 and 2.5 μM BIMI, the PKC inhibitor, resulted in cells producing 0.47 ± 0.03 pg/μg of $VEGF_{xxx}b$, which was significantly greater than cells treated with IGF-1 alone (0.12 ± 0.02 pg/μg, $p < 0.001$) but was not different from treatment with BIMI alone (0.40 ± 0.06 pg/μg, $p > 0.05$, Fig. 1*D*). This was confirmed by Western blot (Fig. 1*C*).

PKC Activation Induces Proximal Splice Site Selection—To determine whether the PKC activation was sufficient to cause proximal splice site selection, cells were treated with 100 nM phorbol myristate acetate (PMA), which is known to induce PKC activation. PMA treatment resulted in a significant increase in VEGF expression as determined by Western blot, but a decrease in $VEGF_{165}b$ expression (Fig. 2*A*). To confirm this quantitatively, ELISA was performed on protein extracted from these cells, and a significant reduction in $VEGF_{165}b$ but increase in total VEGF was seen (Fig. 2*B*). This results in a decrease in the relative $VEGF_{xxx}b$ levels (Fig. 2*C*).

SRPK1/2 Inhibition Prevents the Down-regulation of $VEGF_{xxx}b$ by IGF-1—There are a number of splicing factor kinases that are activated by PKC, including the SR protein kinases SRPK1 and SRPK2 (20, 21). To test the effect of SRPIN340, an inhibitor of SRPK1/2, on IGF-1-mediated down-regulation of $VEGF_{xxx}b$ at the protein and mRNA level, cells were treated with SRPIN340 (10 μM) alone and then in combi-

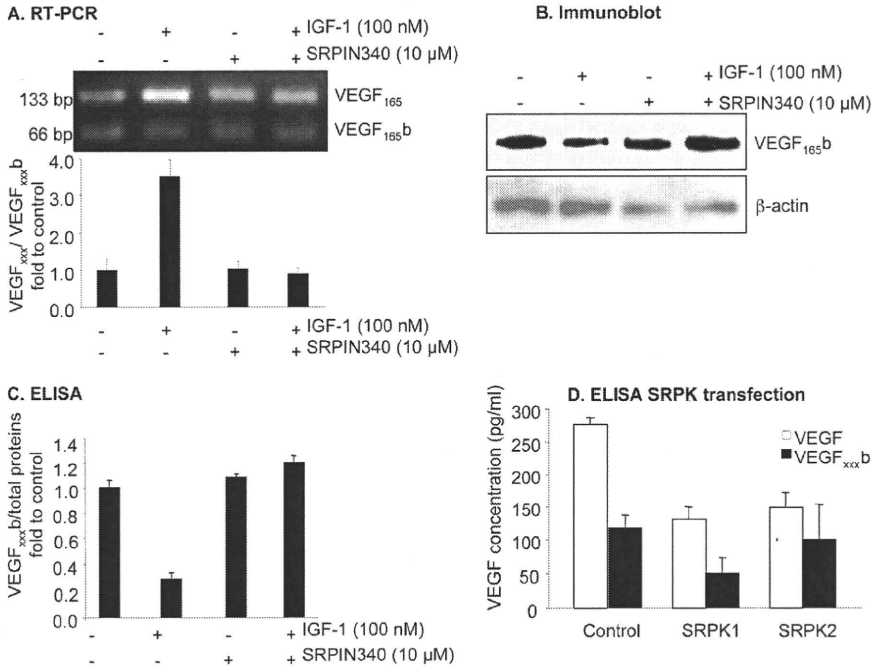

FIGURE 3. **Inhibition of SPRK1/2 by SRPIN340 prevents the down-regulation of $VEGF_{xxx}b$ by IGF.** *A–D*, cells were treated with SRPIN340 (10 μM) alone or in combination with IGF-1 (100 nM). *A*, RT-PCR showed that SRPIN340 reduced the $VEGF_{165}$:$VEGF_{165}b$ ratio at the RNA level. *B*, Western blot demonstrating that SRPIN340 inhibited the IGF-mediated down-regulation of $VEGF_{xxx}b$ expression at the protein level. *C*, ELISA results confirming that SPRIN340 specifically attenuates the IGF-1-dependent down-regulation of $VEGF_{xxx}b$, but did not affect endogenous expression of $VEGF_{xxx}b$. *D*, ELISA of the protein extract shows that SRPK1 transfection reduces $VEGF_{xxx}b$ expression, and total VEGF expression. SRPK2 reduces total expression, but did not affect $VEGF_{xxx}b$ expression.

nation with IGF-1 (100 nM). Amplification of cDNA from podocytes showed that IGF-1 treatment with 10 μM SRPIN340, the SRPK1/2 inhibitor resulted in a relative $VEGF_{xxx}$:$VEGF_{xxx}b$ density of 1.26 ± 0.22, which was lower than treatment with IGF-1 alone (4.84 ± 0.65, $p < 0.01$) but was not different from treatment with SRPIN340 alone (1.45 ± 0.30, $p > 0.05$, Fig. 3*A*). At the protein level, SRPIN340 inhibited IGF-1-dependent down-regulation of $VEGF_{xxx}b$ from 0.12 ± 0.02 pg/μg to 0.50 ± 0.05 pg/μg ($p < 0.001$), but not when SRPIN340 was used alone (0.45 ± 0.01 pg/μg), indicating that SRPK inhibition did not affect endogenous expression of $VEGF_{xxx}b$ (0.42 ± 0.02 pg/μg, $p > 0.05$) (Fig. 3*C*). This was again confirmed by Western blot (Fig. 3*B*). To confirm the involvement of SRPK1 or SRPK2 in the terminal splice site choice, epithelial cells were transfected with expression vectors to overexpress SRPK1 and SRPK2. Fig. 3*D* shows that overexpression of SRPK1, but not SRPK2, resulted in reduced distal splice site selection and hence reduced overall VEGF levels. By itself, it was not sufficient to simply switch the splicing but resulted in inhibition of $VEGF_{165}b$ without increased $VEGF_{165}$. Interestingly, SRPK2 overexpression did not affect $VEGF_{165}b$ production, although it did reduce total VEGF expression.

IGF1 Treatment Resulted in Nuclear Localization of ASF/SF2, which Was Blocked by SPRK1/2 Inhibition—SRPK1 has been shown to phosphorylate ASF/SF2, which we have previously shown to favor proximal splice site selection. To determine whether IGF-1 altered ASF/SF2 localization, podocytes were treated with 100 nM IGF and stained for ASF/SF2. Untreated cells (Fig. 4*A*) contained both nuclear and cytoplasmic ASF/SF2, whereas after treatment with IGF-1, ASF/SF2 localized specifically to the nucleus (Fig. 4*B*). This localization was inhibited by SRPIN340 (Fig. 4, *B versus D*), indicating that IGF1-mediated activation of SRPK1/2 was responsible for the nuclear localization of ASF/SF2. It has previously been demonstrated that ASF/SF2 can be shuttled from the nucleus to the cytoplasm in HeLa cells, but is predominantly nuclear. We therefore investigated ASF/SF2 localization in these and another cell type, HEK293 cells. Fig. 4, *E* and *F* shows that whereas in HEK293 cells there is a strong cytoplasmic localization for the ASF/SF2, in HeLa cells expression is predominantly nuclear, as previously described. This subcellular localization of ASF/SF2 was confirmed by the use of a second ASF/SF2 antibody. Furthermore, high resolution gel electrophoresis showed that whereas podocyte cytoplasmic protein contains a single molecular weight ASF/SF2, an additional higher molecular weight band is seen in podocyte nuclei (data not shown), confirming that in podocytes ASF/SF2 is both cytoplasmic and nuclear. We also investigated $VEGF_{165}b$ mRNA expression in these two additional cell types. Fig. 4*G* shows that HEK cells (with cytoplasmic ASF/SF2) express $VEGF_{165}b$, whereas HeLa cells (nuclear ASF/SF2) only express $VEGF_{165}$. This is consistent with the cytoplasmic location of ASF/SF2 being associated with $VEGF_{165}b$ expression.

ASF/SF2 Requires a 35-nt Region around the Proximal Splice Site of Exon 8 to Bind to VEGF mRNA—To determine whether ASF/SF2 could bind directly to the proximal splice site RNA, we used the MS2-MBP system to pull-down proteins that could interact with the RNA. Fig. 5*A* shows that ASF/SF2 was present both in crude nuclear extract and in the pull-down of nuclear extract incubated with an RNA containing the MS2 binding domain RNA fused to an 88-nt fragment containing the initial 35 nucleotides upstream of exon 8a, the coding sequence of exon 8a, and 35 nucleotides of 3′-UTR. In contrast, less ASF/SF2 was seen in the pull-down of nuclear extract incubated with the mRNA that did not have the 35 nucleotides upstream of exon 8a and did not bind the MS2 binding domain by itself, indicating that ASF/SF2 required a 35-nt fragment of exon 8a upstream of the proximal splice site to most efficiently bind the VEGF pre-mRNA. To determine whether binding of ASF/SF2 was PKC-dependent and whether this was SRPK1-dependent, HEK293 cells were treated with the PKC activator PMA in the presence or absence of the SRPK inhibitor SRPIN340, and then the protein run on an MS2-MBP column

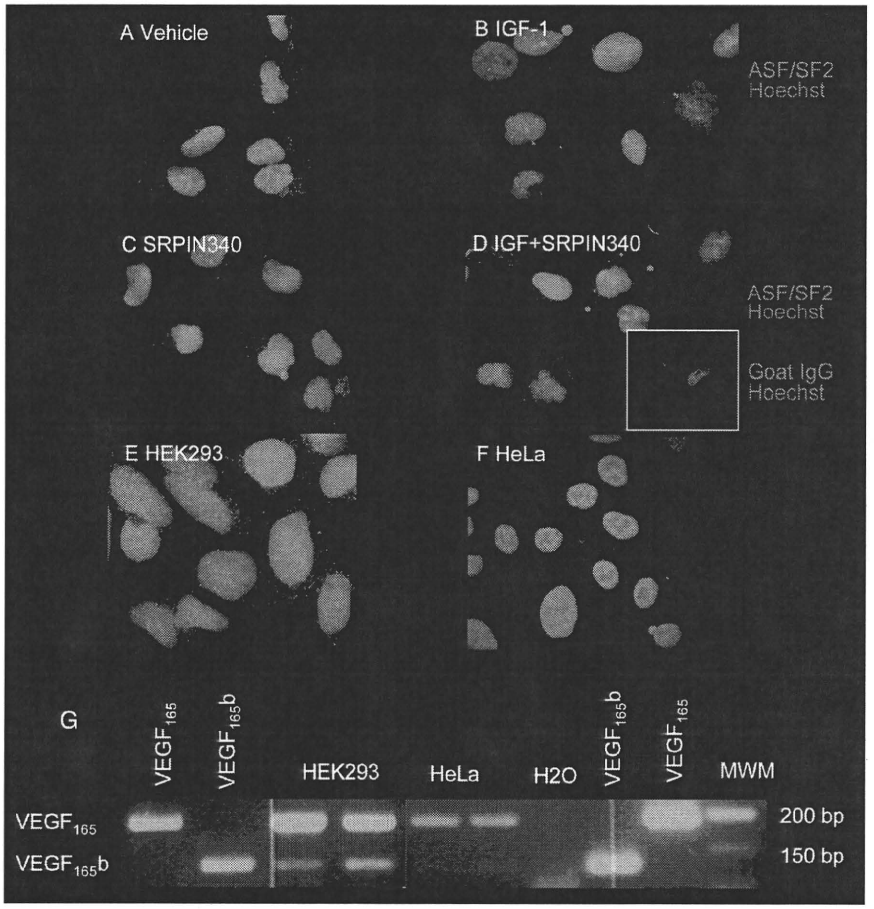

FIGURE 4. **Nuclear localization of ASF/SF2 is increased by IGF-1.** *A–F*, cells were treated with vehicle or IGF in the presence or absence of SRPIN340 and stained for ASF/SF2 and counterstained with Hoechst. *A*, podocytes show expression of ASF/SF2 in the nucleus and in the cytoplasm. *B*, IGF induces nuclear localization of cytoplasmic ASF/SF2. *C*, SRPIN340 by itself does not affect localization of ASF/SF2. *D*, SRPIN340 inhibited this IGF-mediated localization. *E*, HEK cells also show cytoplasmic localization of ASF/SF2. *F*, in contrast, HeLa cells have nuclear ASF/SF2 localization. *G*, RT-PCR of mRNA from HEK cells shows $VEGF_{165}b$ expression, but not in HeLa cells. *MWM*, molecular weight marker.

with the VEGF exon 8 construct. Fig. 5*B* shows that in cells treated with PMA, more ASF/SF2 binds to the VEGF construct than in untreated cells. This increase was inhibited by treatment with 10 μM SRPIN340 or by treatment with the phosphatase PP1. The sequence 35 nucleotides upstream of the PSS contains ASF/SF2 and U2AF65 consensus binding sequences. To determine more precisely the sequence required for ASF/SF2 binding to the RNA, a short sequence upstream of the proximal splice site was mutated (14 nt) or deleted (11 nt) in a plasmid containing just the terminal part of intron 7 and the proximal part of exon 8. Fig. 5*D* shows that the three constructs express the recombinant VEGF RNA (total cell extract, TCE). However, only the wild-type RNA was pulled-down with the ASF/SF2 protein, suggesting that the region we have mutated or deleted is required for ASF/SF2 binding to the VEGF pre-mRNA.

SRPK1/2 Inhibition Inhibits Angiogenesis in a Mouse Model of Retinal Neovascularization—To determine whether the inhibition of proximal splice site selection by blocking SRPK1/2, and hence increased anti-angiogenic $VEGF_{165}b$ production, we used a mouse model of retinal neovascularization where angiogenesis is driven by hypoxia, a process known to favor proximal splice site selection. Injection of SRPIN340 into mouse retina resulted in a significant inhibition of neovascular area of the retina, as well as a significant reduction in ischemic area (Fig. 6, *C*, *D*, and *F*). This resulted in a significant increase in the normally vascularized area, a result that is qualitatively consistent with injection of recombinant $VEGF_{165}b$ into the vitreous in this model (Fig. 6, *E* and *F*). To determine whether VEGF levels were altered by SRPIN340 treatment, mRNA was extracted from the retinae and subjected to Q-PCR for all VEGF isoforms using primers in exon 2 and 3. Treatment of eyes with SRPIN340 made no difference in overall VEGF levels (2.3 ± 0.5% of actin compared with 2.2 ± 2.0%). However, exon 8a containing mRNA was altered from 1.1 ± 0.5 to 0.3 ± 0.2% of actin).

DISCUSSION

VEGF induction by IGF-1 occurs via different signaling pathways including PKC (22) and PI3-K (23–25). There is increasing evidence that transducing components that link the cell surface with the nuclear splicing machinery implicate signaling pathways such as PKC (26), PI3-K (27, 28), or PKB/Akt (29, 30). IGF-1 modulates splicing of VEGF isoforms by preferential use of the PSS to increase expression of pro-angiogenic isoforms (15). Moreover, previously we have shown that ASF/SF2 overexpression preferentially increases usage of the proximal splice site (15) and gives the same effect as IGF-1. SRPK1 has been shown specifically to phosphorylate 12 serines of the RS domain in ASF/SF2 (31), and SRPK2 has been involved in the localization of ASF/SF2 within the nucleus. Thus, in this report, we have investigated the link between the splicing machinery and IGF-1 signaling.

We have shown that the IGF-1-mediated increase in VEGF isoforms using the proximal splice site is inhibited by blocking PKC and SRPK1/2, and that this can be overcome by the use of a PKC inhibitor or mimicked by a PKC agonist or overexpression of SRPK1. This firmly suggests that this kinase cascade is involved in splice site selection in the *VEGF* gene. We have used RT-PCR, ELISA, and Western blotting to investigate VEGF splicing. VEGF isoform mRNA expression depends on transcription, splicing, and degradation of mRNA, and protein expression additionally depends upon translational rate and degradation rate. The finding that the mRNA and protein iso-

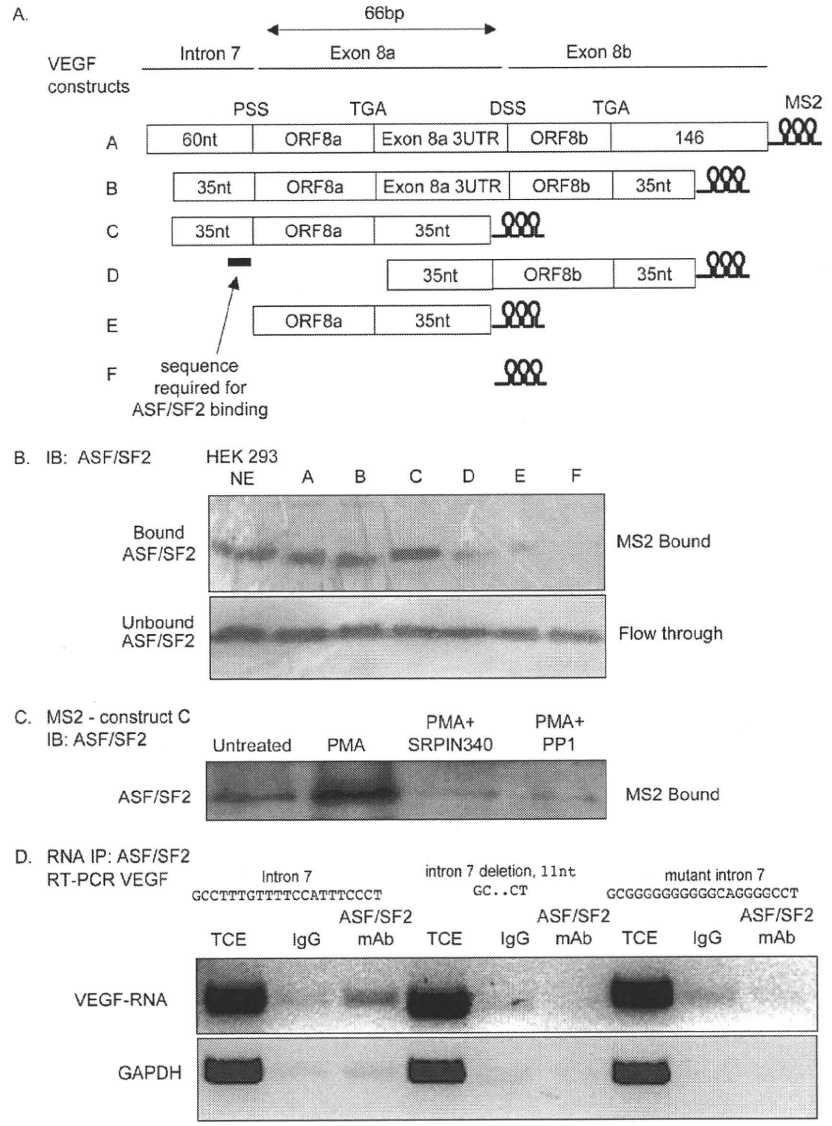

FIGURE 5. **ASF/SF2-1 binds a 35-nt region of VEGF pre-mRNA upstream of the proximal splice site of exon 8.** *A*, constructs were generated containing fragments of the exon 7/exon 8 boundary, fused to a sequence encoding the stem loop structures recognized by the MBP-MS2-binding protein, which can bind maltose. These were transcribed *in vitro*. *B*, Western blot of HEK cell crude nuclear extract (*NE*) or NE incubated with mRNA constructs as above and run over a maltose column to isolate proteins that bind to the RNA constructs and probed with an ASF/SF2 antibody. Whereas mRNA containing the 5′ regions of the intron 7/exon 8 boundary contained ASF/SF2 immunoreactivity, RNA encoding the exon 8 region did not, identifying the binding site for ASF/SF2 in the intron 7/exon 8a boundary. *C*, immunoblot of HEK cell NE of cells treated as shown incubated with the RNA construct C and run over the MS2-MBP column. PMA activation increased binding, and this was blocked by SRPIN340 and phosphatase treatment. *D*, RNA immunoprecipitation of ASF/SF2 in cells expressing constructs with a mutated or deleted intron 7 sequence. The *top* shows RT-PCR of total cell extract (*TCE*) or immunoprecipitated RNA using a nonspecific mouse IgG (*IgG*), or using a mouse monoclonal antibody to ASF/SF2 using primers to detect the VEGF sequence. The *bottom blot* shows the same treatments subjected to GAPDH amplification. The wild-type sequence showed a stronger band in the ASF/SF2 IP, whereas the mutants showed no difference between mouse IgG and ASF/SF2.

have two alternate transcription start sites. Although there is no evidence to date to show that these are differentially used for the different exon 8 isoforms, they do confer different exon 7 inclusion (32). If alternate transcription start sites are used, the splicing machinery would still need to be different in order for the transcription complex to recognize the different exon 8 splice sites. It is possible that these two different isoform families are differentially degraded, and that IGF mediates a decrease in degradation of mRNA encoding the proximal splice site. This is a possibility that we have not as yet excluded. However, the finding that ASF/SF2, a known splicing factor, requires the presence of a specific short sequence in the polypyrimidine tract upstream of the proximal splice site and that ASF/SF2 is induced to nuclear localization by SRPK1 activation and IGF-1 activation strongly suggest that this is a splicing mechanism rather than a degradation mechanism. We have shown that ASF/SF2 requires this sequence, which contains both a U2AF65 and consensus ASF/SF2 sequence, for binding to the VEGF pre-mRNA, but does not demonstrate that this is the sequence it binds to. ASF/SF2 binding to a region upstream of a splice site is generally considered a splicing repressor. There is evidence that SR proteins can interact with sequences upstream of the splice site that act as intronic splicing enhancer or silencer regions (reviewed in Ref. 33); for instance in the *FGFR2* gene mutations in 50% of the sequential 6 nucleotide sequences in the intronic region upstream of the splice site resulted in altered splicing (34). However, an alternative explanation is that ASF/SF2 requires the U2AF65 consensus sequence adjacent to exon 8a to be present in order for it to bind to consensus sequences downstream and repress distal splice site selection, and hence when mutated or deleted DSS repression is lifted resulting in preferential proximal splice site selection. More research is required to pinpoint the exact mechanism of splicing regulation by ASF/SF2.

forms are both altered in a similar way by each intervention suggests that this is an mRNA switch, at least in part. As the mRNAs are generated by alternative splicing it is unlikely that differential isoform production is due to differential transcription, as both isoforms are transcribed from the same promoter region. However, VEGF has been shown to

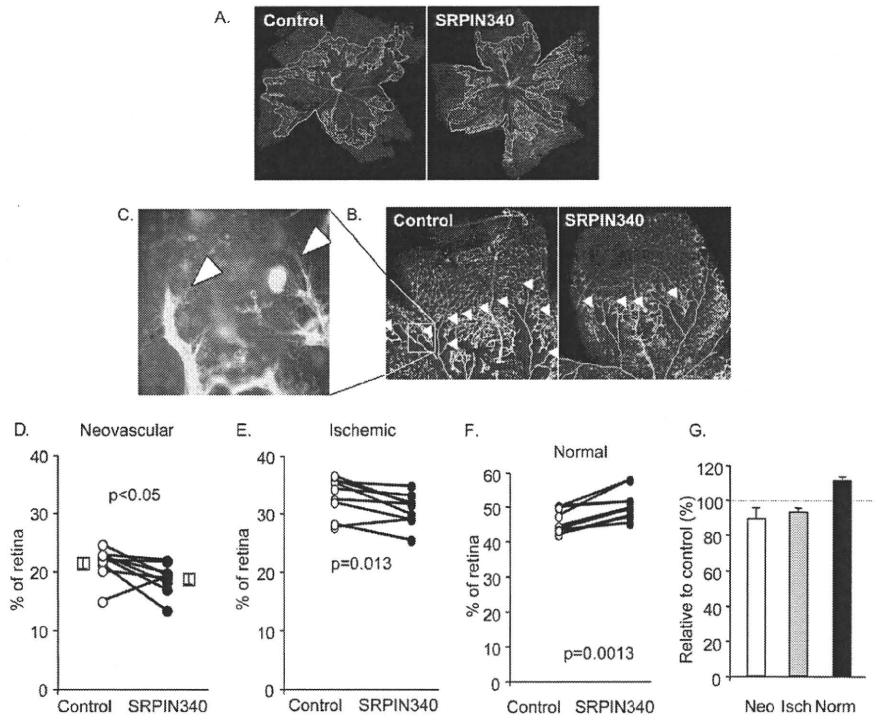

FIGURE 6. **Neovascularization induced by hyperoxia is inhibited by a single dose of SRPK inhibitor, SRPIN340.** *A*, low power fluorescence micrograph of FITC-labeled lectin staining of retinal whole mounts with areas of NV (*white*) and ischemic (*orange*) outlined. *B*, higher power view of a single retinal quadrant, with angiogenic areas highlighted by *arrowheads*. *C*, high power view of retinal angiogenic area showing sprouting endothelial cells. *D*, quantification of neovascular areas shows a small but significant inhibition by a single injection of 1 μl of 10 μM SRPIN340 1 day after removal from oxygen. *E*, ischemic area was also reduced in these mice. *F*, normal area was consequently increased. *G*, data shown as relative to control, uninjected contralateral eye. *Neo*, neovacular; *isch*, ischemia; *Norm*, normal.

SRPK1 seems to be a relatively new target for future cancer therapies but is receiving more attention recently as higher expression of SRPK1 has been observed in breast and colonic tumors, and its increased expression is associated with the grade of a tumor (50). Moreover, it has been shown that known anticancer drugs such as gemcitabine and cisplatin increase cell apoptosis with a much stronger effect when phosphorylation of SR proteins was inhibited by using siRNA against SRPK1 (51). SRPK2 is able to bind and phosphorylate acinus, an SR protein, and moves it from nuclear speckles to the nucleoplasm, resulting in the activation of cyclin A1 (52). Moreover, overexpression of acinus or SRPK2 increased leukemia cell proliferation. SRPK2 and acinus were also overexpressed in human acute myelogenous leukemia patients and correlate with elevated cyclin A1 expression levels (52). These two kinases are able to phosphorylate the splicing factor, ASF/SF2 and all these components are involved in the choice of the PSS in VEGF. The inhibitor of SRPK1/2 kinase, SRPIN340 prevents the down-regulation of the $VEGF_{xxx}b$ isoforms. Moreover, SRPK1 and SRPK2 are known to phosphorylate the ASF/SF2 splicing factor with high specificity (21, 31, 53). These results indicate that an overactivity of SRPK1 can cause phosphorylation of ASF/SF2. However, SRPKs have other targets, including those known to up-regulate $VEGF_{xxx}b$ such as SRp55 (15), and the contribution of SRp55 phosphorylation to IGF-mediated effects (perhaps by inhibiting its binding to the distal splice enhancer region) cannot be ruled out. It thus appears likely that SRPK1-mediated phosphorylation of ASF/SF2 could support an activation of the PSS and increased production of pro-angiogenic isoforms.

The overexpression findings, however, suggest that whereas SRPKs are necessary, they are not sufficient for proximal splice site selection. Thus these findings indicate that SRPK1 inhibitors may be potentially anti-angiogenic, and to that end we set out to investigate this in a model of angiogenesis in the eye. A single dose of SRPIN340 resulted in significant inhibition of angiogenesis and increased normal vascularization. Whereas, we have not measured $VEGF_{165}b$ levels in these eyes, there is a discrepancy between total and exon 8a-containing isoforms that is most likely a result of altered splicing. The angiogenesis is known to be mediated by pro-angiogenic VEGF and can be inhibited by anti-angiogenic $VEGF_{165}b$ (18); thus, allowing us to draw a parallel between anti-angiogenic splice forms and inhibition of splice factors that cause pro-angiogenic splicing in

It is still not clear if the IGF-1 system plays a direct role in the growth of new blood vessels. However, there are increasing examples that IGF-1 indirectly increases angiogenesis by up-regulation of VEGF (22, 25, 35). Moreover, IGF-1 induces angiogenesis in the rabbit cornea (36) and stimulates migration, proliferation (37), and tube formation of human endothelial cells (38). IGF-1 is also widely implicated in pathological angiogenesis. Expression of IGF-1 was increased in the vitreous of patients with diabetic retinopathy (39). There is a positive correlation between elevated VEGF-A and IGF-1 in different types of cancers such as colorectal cancer (40), breast cancer (41), and head and neck squamous cell carcinomas (25).

Moreover, the *SFRS1* gene, encoding ASF/SF2, fulfills the criteria of a proto-oncogene (42). Overexpression of ASF/SF2 in immortalized rodent fibroblasts resulted in formation of high-grade sarcomas after injection into nude mice (43). Knock-down of ASF/SF2 in lung carcinoma, which has high expression of that molecule, inhibited tumor formation in nude mice (43).

There are increasing examples that manipulation of the splicing machinery can be used as new therapeutic targets (44). Small molecules that can target splicing factors and kinases involved in splicing are promising candidates for drugs (17, 45–47). Alternatively, the use of antisense oligonucleotides such as morpholinos, which can bind to the specific splice sites to modulate aberrant splicing has been investigated (48, 49).